ULB UNIVERSITÉ LIBRE DE BRUXELLES

Bruface Brussels Faculty of Engineering

Vrije Universiteit Brussel

Implementation of an FPGA-based calibration procedure at the detector level for the future high-luminosity phase of the CMS

Dewitte Hugo

Master thesis submitted under the supervision of
Prof. Frédéric Robert

The co-supervision of
Prof. Gilles De Lentdecker

In order to be awarded the Master's Degree in
Electronics and Information Technology Engineering

Academic year
2015-2016

Hugo Dewitte - Electronics and Information Technology Engineering - 2015/2016

Implementation of an FPGA-based calibration procedure at the detector level for the future high-luminosity phase of the CMS.

Abstract

The GE1/1 project, which started in 2010, has for objective to install triple-GEM detectors -along with their acquisition chain- in the Compact Muons Solenoid (CMS), one of the 4 experiments of the Large Hadron Collider (LHC). This master thesis is a contribution to the development and the commissioning of the acquisition electronics (DAQ) of the project, and more precisely of the VFATs, the first chips in this chain. After the description of the LHC and CMS, the GE1/1 project and its acquisition electronics, this master thesis presents the implementation of a calibration procedure for the VFATs. To do so, the thesis starts by developing firmwares and software routines which, in an automated way, scan the VFATs, collect a maximum of information and set the registers depending on the results, in order to ensure an optimized functioning of the chips during their operations. Since the GE1/1 project is still under development, the second part of the master thesis presents a series of studies performed with the calibration procedure on existing prototypes of the detector and its acquisition electronics. These systematic studies have allowed to observe several issues related to unexpected noise, and helped to solve most of them. Finally, the master thesis discusses the VFAT noise when the chip is connected and not connected to the CMS triple-GEM detector, and compares the measurement with the theoretical prediction. This study highlights the dependence of the noise on the detector capacitance.
Keywords: VFAT, GE1/1 Project, CMS, LHC, Triple-GEM, Acquisition Electronics (DAQ).

Hugo Dewitte - Electronics and Information Technology Engineering - 2015/2016

Implementation of an FPGA-based calibration procedure at the detector level for the future high-luminosity phase of the CMS.

Résumé

Lancé en 2010, le projet GE1/1 a pour objectif d'intégrer en 2020 des détecteurs Triple-GEM - ainsi que leurs chaines d'acquisition de données - au complexe de détecteurs du Compact Muons Solenoid (CMS), une des 4 expériences du Large Hadron Collider (LHC). Ce mémoire de fin d'étude est une contribution au développement de l'électronique de la chaine d'acquisition (DAQ) du projet, et plus particulièrement de la VFAT, le premier module de cette chaine. Après une description du LHC, du CMS, du projet GE1/1 et de son électronique d'acquisition, ce mémoire présente l'implémentation d'une procédure de calibration des VFATs. Pour cela, le travail commence par développer des firmwares et des routines de software qui, de manière automatisées, scannent les VFATs, récoltent le maximum d'informations et définissent leurs registres en fonction de ces résultats pour leur assurer un fonctionnement optimisé lors de leur utilisation. Etant donné que le projet GE1/1 est toujours en phase de développement, la seconde partie de ce MFE présente une série d'étude réalisée à l'aide de la procédure de calibration sur le prototype du détecteur et de sa chaine d'acquisition. Ces études systématiques ont permis d'observer plusieurs problèmes liés à des bruits électroniques non suspectés, et ont aidé à en résoudre la majorité. Finalement, le mémoire traite du bruit de la VFAT lorsque celle-ci est connectée ou non au détecteur CMS triple-GEM, et compare les résultats avec les prédictions théoriques. Cette étude permet de mettre en avant la dépendance du bruit en fonction de la capacité du détecteur.

Mots-clés: VFAT, Projet GE1/1, CMS, LHC, Triple-GEM, Electronics d'Acquisition (DAQ).

Hugo Dewitte - Electronics and Information Technology Engineering - 2015/2016

Implementation of an FPGA-based calibration procedure at the detector level for the future high-luminosity phase of the CMS.

Samenvatting

Het project GE1/1 werd gelanceerd in 2010 met als objectief om tegen 2020 Triple-GEM detectoren - samen met hun data aankoopketen – te integreren in het detectoren complex Compact Muons Solenoid (CMS), een van de 4 Large Hadron Collider (LHC) experimenten. Deze master thesis vormt een bijdrage aan de ontwikkeling van de elektronica van de aankoopketen (DAQ) van het project en meer in het bijzonder van de VFAT, de eerste module van deze keten. Na de beschrijving van de LHC, de CMS, het GE1/1 project en zijn aankoopelektronica, stelt deze master thesis de implementatie van een calibratieprocedure van de VFAT's voor. Daarom begint het werk met de ontwikkeling van firmwares en van de softwareroutines die op een geautomatiseerde manier de VFAT's scannen, het maximum aan informatie verzamelen en hun registers definiëren in functie van deze resultaten om een optimaal functioneren te verzekeren tijdens het gebruik. Omdat het GE1/0 project zich nog steeds in een ontwikkelingsfase bevindt, toont het tweede luik van de master thesis een serie studies gedaan met behulp van de calibratieprocedure, uitgevoerd op het prototype van de detector en van de aankoopketen. Deze systematische studies hebben het mogelijke gemaakt om verschillende problemen in verband met onverwachte elektronische ruis vast te stellen en om het merendeel van deze problemen op te lossen. Als laatste onderwerp behandelt deze thesis de VFAT ruis, terwijl deze al dan niet verbonden is aan de CMS triple- GEM en vergelijkt de resultaten met de theoretische voorspellingen. Deze studie toont aan dat de ruis afhankelijk is van de capaciteit van de detector.

Sleutelworden: VFAT, GE1/1 project, CMS, LHC, Triple-GEM.

Acknowledgments

I would like to thank my supervisors, Frédéric Robert and Gilles De Lentdecker, for their invaluable guidances in the design and the redaction of this thesis.

I am also grateful to Thomas Lenzi and all members of the IIHE department for their numerous advices and the friendly working environment they have provided.

I finally thank my relatives, and especially my brother, for their support and patience in the review of this work.

Contents

Introduction

The CERN is the biggest research center of particle physics in the world, and within it resides the biggest machine ever built by mankind, the LHC, a 27km long particle collider. The LHC accelerates protons at an energy of several TeV and makes them collide in 4 points, one of them being a 14000 tons cylindrical shaped detector, the CMS experiment. Composed of thousands square meters of detector layers, it observes the gargantuan quantity of particles created by these collisions at a frequency of 40MHz.

The life of the LHC is interspersed by shutdown phases for maintenance and upgrade. The second shutdown phase of the LHC, which will take place in 2018, will allow, among other things, to upgrade the CMS experiment and enhance its performances. It is in that context that the project to which the master thesis is related takes place. The GE1/1 project, as it is called, has started in 2010 and has for objective to develop gas detectors equipped by triple-GEM technologies, along with there acquisition electronics, under the constraints of efficiency, precision and radiation hardness required for CMS.

This project has been partially entrusted to the Inter Institute of High Energy (IIHE) in Brussels, a ULB-VUB collaboration. It is in that department that the master thesis has been realised. This master thesis focuses on the acquisition electronic of the project and more precisely the VFATs, the first chip in the acquisition chain, whose about 3500 copies will be placed inside the CMS.

In each VFAT, there are many control registers that need to be set to ensure a correct behaviour of the chip, depending on the fabrication fluctuations and the condition of operation. This master thesis develops a calibration procedure that will scan a large spectrum of information on a VFAT and, depending on the results, correctly calibrate its different registers.

To start, the different tools used for extracting the information from the VFATs are developed or adapted. Then, the first part of the master thesis is devoted to the implementation of the calibration procedure in python using these tools. The python script, controlling the VFATs via a FPGA-Based board, has been automatized to reduce the amount of work and to ensure a common tuning procedure for all the VFATs.

Finally, since the project is still in research and development, the second part of the master thesis runs the script on the in-developement setup and uses the results to characterize the VFATs. This characterization will make the difference between a good and a bad VFAT, and, in the case of a bad VFAT, find or confirm the problems and help to solve them.

The master thesis starts by introducing the context with the presentation the LHC and CMS (Chapter 1), the project and its technologies (Chapter 2) and the acquisition electronics (Chapter 3). Then the development of the tools and their use is detailed (Chapter 4). Finally, the two parts of the master thesis are detailed: the calibration procedure with its results (Chapter 5) and the VFAT analysis in the different situations with the problems and their solutions (Chapter 6 and 7).

Chapter 1

LHC and CMS

1.1 The Large Hadron Collider

The Large Hadron Collider is the largest and most powerful particle collider in the world. Inside the LHC, two beams of hadrons (protons or ions of lead) are accelerated in opposite directions. These beams collide in four particle detectors: ATLAS, CMS, ALICE and LHCb (Figure 1.1) [1, 4, 10]. The collisions produce unstable high mass particles and their decay can be observed in the detectors. These observations have, for instance, led to the discovery of the Brout-Englert-Higgs boson by the CMS and the ATLAS detectors [5].

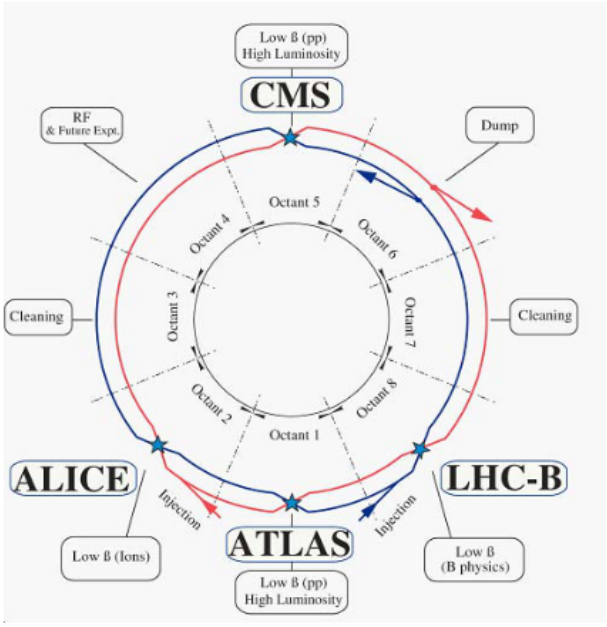

Figure 1.1: Diagram of the LHC and the repartition of the main detectors. The two beams and their collision points are also visible [10]

.

In this section, the relevant characteristics of the LHC will be presented as well as its calendar, from the beginning of its life till its programmed end.

1.1.1 The LHC characteristics

In the context of the particle colliders, the relevant characteristics of the LHC for the experiments are the luminosity and the energy of collision. They are briefly introduced here.

Luminosity

The luminosity characterizes the number of collisions inside a collider. Rather than being uniformly distributed in the beam, the protons are bunched together in packets. In each beam, there are around 2000 packets of 10^{11} protons at the same time. The packets of the two beams are crossed in the center of the detectors at a frequency of 40 MHz, but not every proton within a packet will collide. The number of collisions per second (N_c) in a collider can be defined by [10]:

$$N_c = \mathcal{L}\sigma \tag{1.1}$$

where $\mathcal{L}$ is the instantaneous luminosity and σ the cross section. Typically, $\mathcal{L} = 10^{34} cm^{-2} s^{-1}$ and $\sigma = 10^{-25} cm^2$ in the CMS. Thus, there are only around 25 protons that collide at each packet crossing, the remaining ones continuing their way in the LHC. The luminosity can also be expressed in "integrated luminosity". It is the integral of the instantaneous luminosity over the duration of operation and it is expressed in inverse femtobarn ($fb^{-1} = 10^{39} cm^2$) [11]. This value is often used to express the amount of data collected by the experiments.

Energy of Collision

At a collider, the energy that really matters is the energy in the center of mass system. In that case, the laboratory system is also the center of mass system and all the energy is useful. This energy is expressed in eV and defines a single collision. The LHC has been designed to work with a nominal energy of 14 TeV. Today, it is running at an energy of 13 TeV for proton-proton collisions. The energy of collision, along with the luminosity, are increased during the life of the LHC[1].

1.1.2 Calendar of the LHC

Between its start in 2010 and its predicted end of life in 2035, the LHC alternates between periods of data acquisition and periods of long shutdowns (LS). These long shutdowns are used to carry out repairs, upgrade the system and add new features to the LHC. A calendar of these periods is presented on figure 1.2. The estimated augmentations of the instantaneous and the integrated luminosities are also presented on the figure. The calendar is divided in two phases: the phase 1 from 2010 to 2023 and the phase 2 from 2023 to 2035.

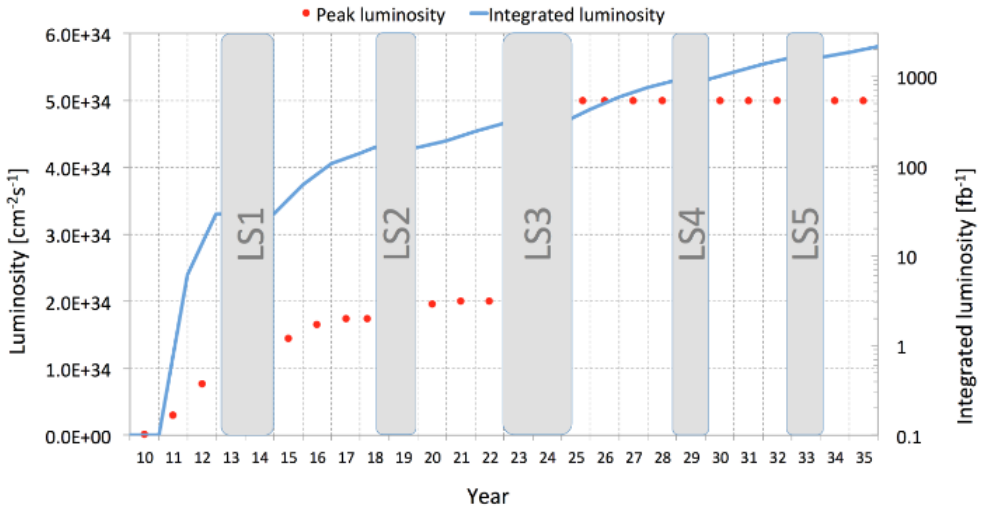

Figure 1.2: Calendar of the different periods of the LHC [11].

Phase 1

Phase 1 lasts from 2010 to 2023. During this phase the luminosity along with the energy of collision will be progressively increased. It will be divided into 3 periods, each time separated by periods of shutdown. During the redaction of this master thesis, the LHC is currently in its second period. The GE1/1 project is planned to be integrated inside the CMS during the next shutdown phase, between 2019 and 2020. It will thus start its measurements during the last period of the first phase - that is, in 2020.

Phase 2

Phase 2 will last from 2022 and 2035. It will start with a very long shutdown phase of more than 2 years and is also composed of 3 periods separated by shutdowns. During this second phase, the LHC will enter a phase of High Luminosity (HL-LHC). The luminosity will be increased by a factor of 2.5 compared to the last periods of phase 1 and will be maintained constant during the phase 2.

1.2 The Compact Muon Solenoid (CMS)

The Compact Muon Solenoid (CMS) is one of the four main detectors around the LHC. As its name suggests, one of the main tasks of the CMS experiment is the detection and the study of the muons. An overview of its structure is presented on figure 1.3. It is a giant cylinder of 28.7 m in length and 15 m of diameter for a weight of 14000 tons. It is constructed like a barrel closed with two endcaps. This disposition, clearly visible on figure 1.3, ensures an optimal coverage of the collision point.

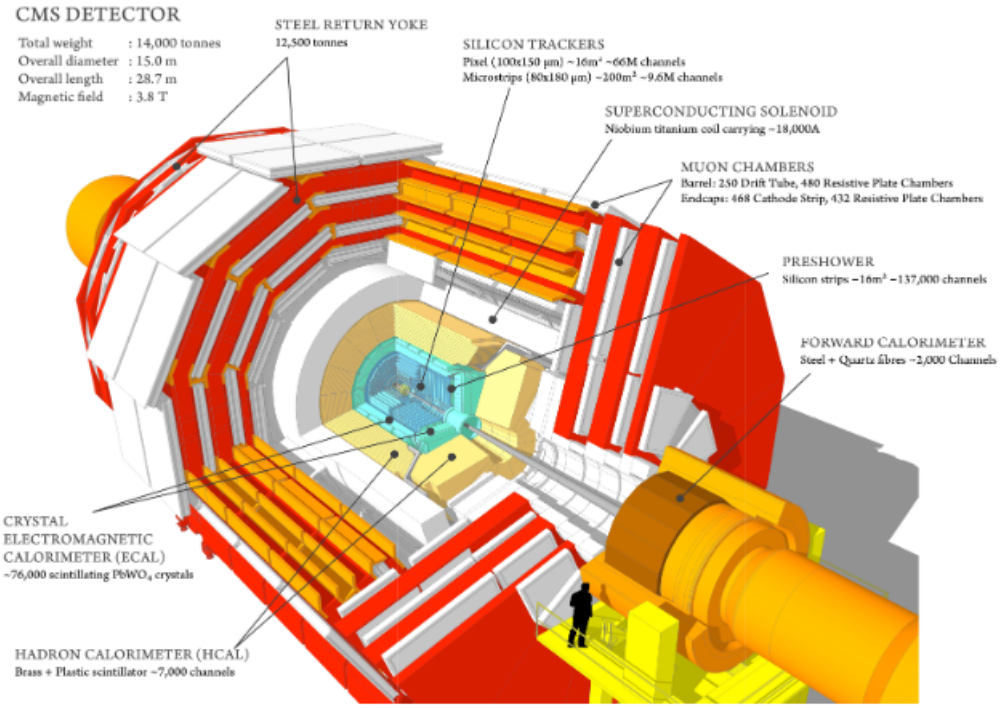

Figure 1.3: Schematic 3D representation of the CMS Experiment [2].

In this section the different techniques of detection inside the CMS experiment will be presented. Then, the disposition of the different detection layers will be detailed. Finally, the system of trigger, an essential feature of CMS, will be described [11, 13].

1.2.1 Detection principles inside the CMS

During a collision, around 1000 particles are created and the CMS detector has to be able to identify them. To do so, CMS is equipped with many sub-detectors. They can be sorted in two categories: the Calorimeters, that measure the energy produced by a particle, and the Trackers that determine the momentum of the particles by estimating their trajectory in a magnetic field. Both are presented in the following subsections.

The Calorimeters

A calorimeter is a device that absorbs the totality of a particle's energy and produces a signal proportional to the energy absorbed. The calorimeter is thus a thick strip of a certain medium that interacts with the studied particles. In CMS, there are two types of calorimeters: the electromagnetic calorimeters (ECALs) designed to measure the energy of the photons, the electrons and positrons, and the hadronic calorimeters (HCALs) designed to measure the energy of the hadrons.

In an electromagnetic calorimeter, high energy electrons (or positrons) lose most of their energy through bremsstrahlung, that is they irradiate a high energy photon. These bremsstrahlung photons

can, in turn, convert to electron-positron pairs, which can radiate more photons, creating an electromagnetic "shower". The shower particles excite the material atoms, a crystal of $PbWO_4$ in CMS, which emit low energy photons detected by photo-detectors located at the end of the crystals.
Similarly, in a hadronic calorimeter, hadrons can deposit energy in matter through a series of successive nuclear interaction. Eventually, the resulting low energy particles deposit their energy by ionizing atoms within the medium. Therefore, hadronic calorimeters often contain a uninstrumental absorber material that is interspersed with active sampling devices to sense the energy of the developing shower. In CMS, the HCAL absorbing layer is in brass and the measuring layer in scintillator plastic.

Since, in most materials, the mean free path for nuclear interaction is substantially greater than for electromagnetic interactions, hadronic calorimeters are physically thicker than electromagnetic calorimeters.

The Trackers

The trackers are used to fulfil two roles: to measure the momentum of a particle and to estimate the collision point.
To determine the trajectory of the particle, the tracker is composed of multiple layers. Each one measures the coordinates of the passing particles. In opposition with the calorimeters that were designed to stop the particles, the measurements in the tracker need to be the less intrusive possible in order to preserve the measurements of the next layers of detection. Thin semi-conductor or gas detectors are well fitted for this task. The trajectory of a particle can then be reconstructed from all the measured points. This is not an easy task due to the limited spatial resolution (also called granularity) of the tracker and powerful algorithms are therefore needed to determine the trajectory on the base of the measured points, taking into account the granularity. Then, knowing the magnetic field inside CMS and the trajectory of a particle, its momentum can be computed using the well known Lorentz law.
Once several trajectories from a collision are determined, they can be extrapolated to find the collision point.

1.2.2 Detector Layer disposition inside CMS

CMS is an assembly of these calorimeters and trackers. They are arranged in successive layers as presented in the cross section on figure 1.4. The different layers are detailed from the inside to the outside of CMS [1, 4, 11].

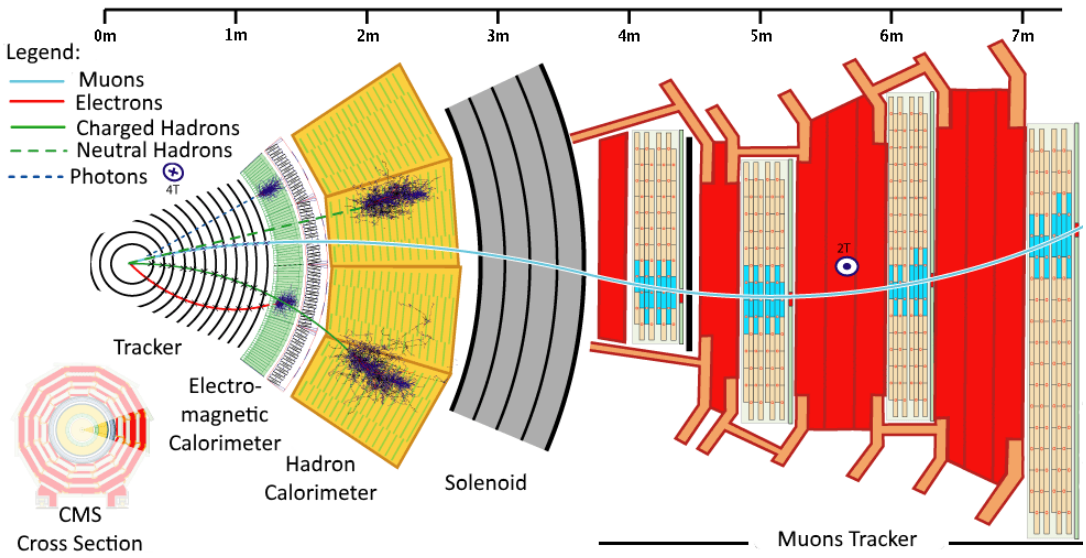

Figure 1.4: Cross section of one sector of the CMS barrel.

From the collision point outwards, the first layer of the CMS is a **silicon tracker**. It is designed to precisely determine the collision point and to measure the impulsion of the charged particles.
It is followed by a **Electromagnetic Calorimeter, ECAL**, designed to measure the energy of the electrons and the photons. Its detections of the photons are essential since, unlike electrons, photons cannot be observed in the internal tracker due to there neutrality.
The electromagnetic calorimeter is directly followed by the **Hadron Calorimeter, HCAL**. This calorimeter is designed to measure the energy of hadrons (n,p,π,k,...).
All these layers are placed inside the **solenoid magnet**. It is maintained to a temperature of 4.5 ^oK to ensure super-conductivity and to produce a magnetic field of 3.8T.
Outside the magnet, only the neutrinos and the muons remains because they are the only ones penetrating enough to pass through all the previous layers. **The muon tracker or spectrometer** is thus placed there. This tracker is designed to realise three tasks: detect the muons, determine their impulsion and participate to the creation of the trigger signal (see next subsection). Due to its distance from the center of CMS, the surface covered by the muon tracker is about 25000 m^2. Gas detectors have therefore been chosen over semi-conductor, contrary to the first layer tracker, due to their capacity to cover a bigger area for a smaller cost. Such a succession of detector layers is also present in the endcaps which close the CMS barrel. The detector studied in this master thesis are planned to be used in the upgrade of the muon tracker in the endcaps.

1.2.3 System of trigger in the CMS

Once the LHC runs at its nominal luminosity, almost 10^9 proton-proton collisions happen every second in the CMS and this number will increase during the life time of the LHC. As it is impossible to collect all the data produced by these billions of collisions, a system of selection is implemented to determine the pertinent events. The pertinence on an event depends on the experiment or the particles observed. During the process of creation of theoretically predicted particles, the charge, the energy or the mass

is defined. It is thus possible to predict a pattern inside the CMS for these particles. This pattern can then be used to select only pertinent events. Such a system is called a trigger system and, in CMS, it is divided in two levels of selection: the Level-1 trigger (LV1) and the High Level Trigger (HLT). Together, they reduce the frequency of data acquisition from 40 MHz to 100Hz. Both are presented on figure 1.5 and described in following subsections [4, 11, 13].

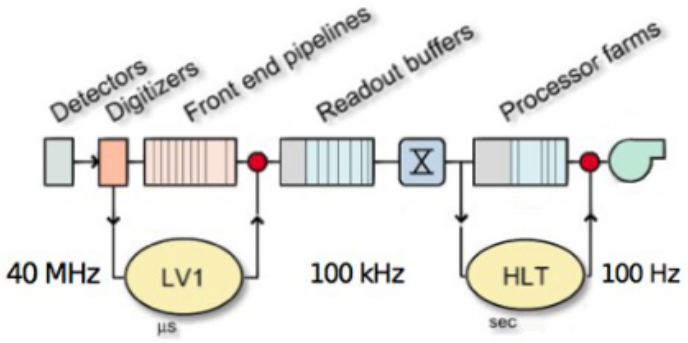

Figure 1.5: Schematic view of the CMS trigger system [19].

LV1

The objective of the first trigger system is to divide the frequency by 400. The system has 3.2 μs to take a decision and a new decision has to be taken every 25 ns to avoid congestion in the system. Given this high time constraint, only a part of the data of the trackers and the calorimeters is used (e.g. data with a smaller granularity) [9]. During the decision process, the tracking data are stored on FIFO RAM memory on the detector. If the data are judged pertinent, a Level-1 acceptance signal is transmitted back and all the data are extracted and sent to the next selection level, the HLT. If they are not judged pertinent, the data are never extracted and end up being erased from the FIFO memory by more recent data [3].

HLT

The HLT receives the selected data by the LV1 at a frequency of 100kHz. Each data packet represents 1.5 MB. Since the time constraint is much less restrictive (around 1s), more powerful algorithms, taking into account the totality of the data, are used. These algorithms allow to reduce the frequency of pertinent data acquisition to several hundreds of Hz [19].

Chapter 2

The GE1/1 project

The GE1/1 project is developing a new gaseous detector technology, destined to be added at the existing muons tracker in the CMS endcaps during the next long shutdown in 2018. In this chapter, a brief overview of the actual technologies inside the muon tracker is presented. Then, the GE1/1 is described with its constraints and objectives. Finally, a mechanical description of the detector prototype is done.

2.1 Actual Technologies inside the muon tracker

In its actual disposition, three types of gas detectors are used inside the muon tracker: the Drift Tubes (DTs), the Cathode Strip Chambers (CSCs) and the Resistive Plate Chambers (RPCs). The DTs are placed in the central barrel region, while the CSCs are placed in the endcaps region and the RPCs in both [4]. This disposition can be observed on figure 2.1, which represents a longitudinal cross-section of CMS with the different layers of the muon tracker. Each layer is separated by a return yoke, which produces a constant magnetic field of 2T in the muon tracker.

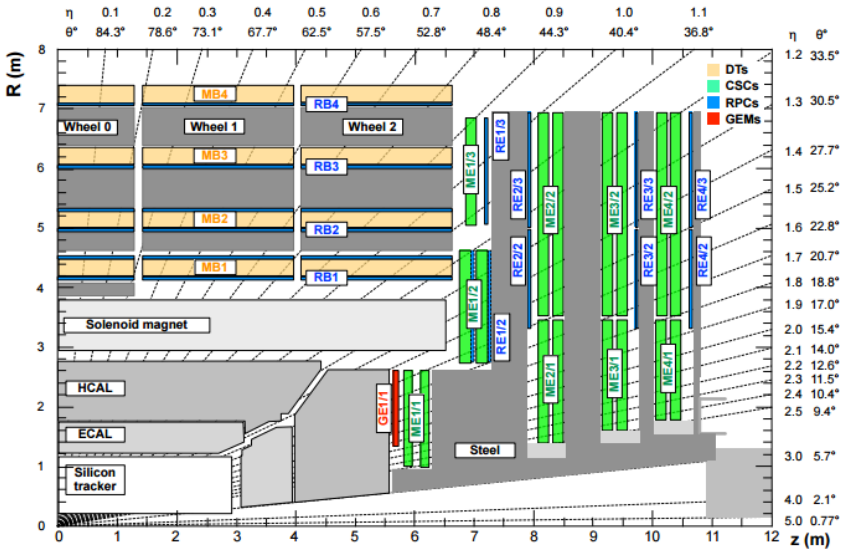

Figure 2.1: Transverse section of the CMS detector showing the present muons system including RPCs, DTs and CSCs and the location of the GE1/1 project [6].

A convention is used to name the different parts of the muon tracker. A first letter describes the type of detector, and a second one the region of the detector (E for Endcap and B for Barrel). Then, two numbers describe precisely the position inside the region, as shown for the endcap on figure 2.1.

2.2 Introduction to the GE1/1 project

2.2.1 Justification of the GE1/1 project

The location of the GE1/1 project inside the CMS endcap is shown on figure 2.1. Initially, this location was reserved for RPCs detectors. However, the rise in the luminosity of the LHC has increased the constraints in CMS and the predicted particle rate in this position ($5kHz/cm^2$) has become too high for the RPCs capabilities [4]. The implementation of the RPCs had therefore to be abandoned for this location in the endcaps, leading to a reduction in the layers and unused space. The GE1/1 project has been designed to fill this gap, with more adapted detectors than the RPCs. The project has two goals. First, it should improve the impulsion determination of the muons. The augmentation of the luminosity will increase the number of particles produced at each proton bunch crossing. An improvement in momentum resolution is therefore necessary to maintain the data acquisition frequency at 100 kHz after the LV1. Secondly, the project should also offer a redundancy of detection to counteract the degradation of the other detectors predicted during the HL-LHC phase, to keep the high efficiency of the overall system.

2.2.2 Constraints on the GE1/1 project

In this subsection, the most notable constraints on the project are detailed.

- **Geometry:** The detector installed in CMS has to cover the totality of the zone without blind spots. Moreover, it should fit in the zone left by the RPCs removal, that is not thicker than 10 cm.
- **Detection rate:** During the HL-LHC phase, the particle rate at the GE1/1 detector is predicted to reach 5 kHz/cm^2. To ensure a safety margin of 2, the detector should be able to correctly work with a particle rate of 10 kHz/cm^2.
- **Efficiency:** The efficiency of the detector is expected to reach 97%. The use of a double layer of detector will increase this efficiency to 99.9%.
- **Spatial resolution:** The spatial resolution should be better than 250 μ rad in ϕ, with ϕ the polar angle within CMS.
- **Time resolution:** The time resolution of the new detector should be better than 10 ns.
- **Radiation hardening:** The detector should resist to the radiation level received during its complete lifespan. This level is expected to be $100mC/cm^2$. Considering a safety factor of 2, the detector should resist to a total radiation dose of $200mC/cm^2$.

To fill these constraints, triple-GEM detectors have been selected. After a brief overview of existing projects using triple-GEM detectors, their principle of operation is presented.

2.2.3 GEM detector in other projects at CERN

The GE1/1 project is not the first project to implement triple-GEM at CERN. Three other projects have already successfully implemented it: COMPASS [1], LHCb [8] and TOTEM [9]. Even if the three projects use smaller GEM detectors, their performances are very encouraging for the possibility to meet the constraints presented in the previous section [6].

2.3 Mechanical description of the GE1/1 detector

The detectors are located just behind the forward hadron calorimeters. Figure 2.2 shows a 3-D representation of the CMS endcap with the detectors in pink and blue. Each detector has a trapzoidal shape and covers 10^o in ϕ [6, 11, 17].
Each sector is actually made of 2 triple-GEM detectors back-to-back to form a super-chamber. The first level trigger effectuates a logic OR between the results of the two independent detectors.
For space constraints, two super-chambers with different length alternate, as it can be seen on figure 2.2. Each super-chamber has the same small side width of 234.31mm. The lengths are respectively 1209mm and 1060.84mm [6].
To cover the complete ring, 36 prototypes are needed. Since there is 2 layers of detectors and 2 endcaps, a total of 144 detectors will be placed in the CMS, representing a surface of around 25 m^2.

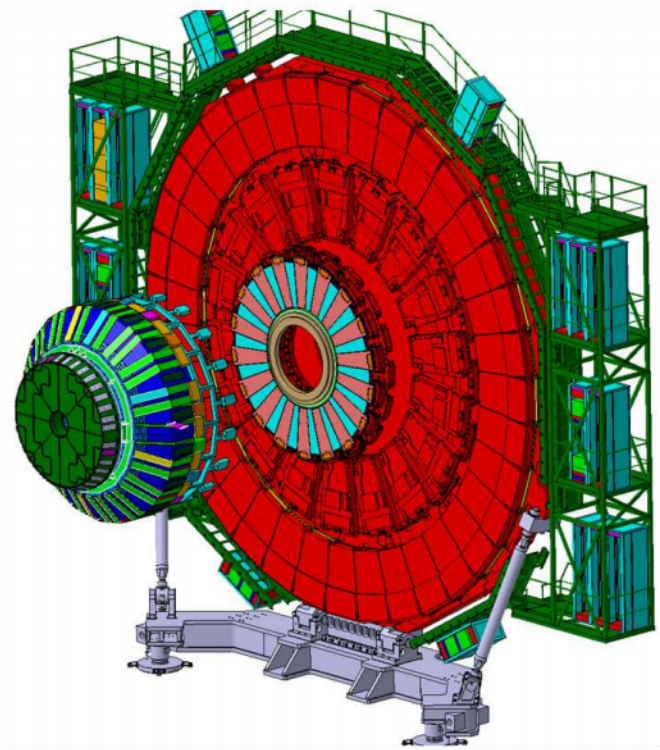

Figure 2.2: First CMS endcap station where the inner ring is equipped with 18 long (pink) and 18 short (blue) triple-GEM detectors [6].

Figure 2.3 presents an exploded view of the detector in its different layers. From the bottom to the top: the triple-GEM detector which is composed of the Drift electrode (pink), three GEM foils (light blue) and the readout board (dark blue), then the GEB (red) on which is plugged the acquisition electronics. Each of these layers is detailed in the following sections, except for the acquisition electronics that will be presented in a separated chapter. A more detailed decomposition of the detector is presented in the appendix A.

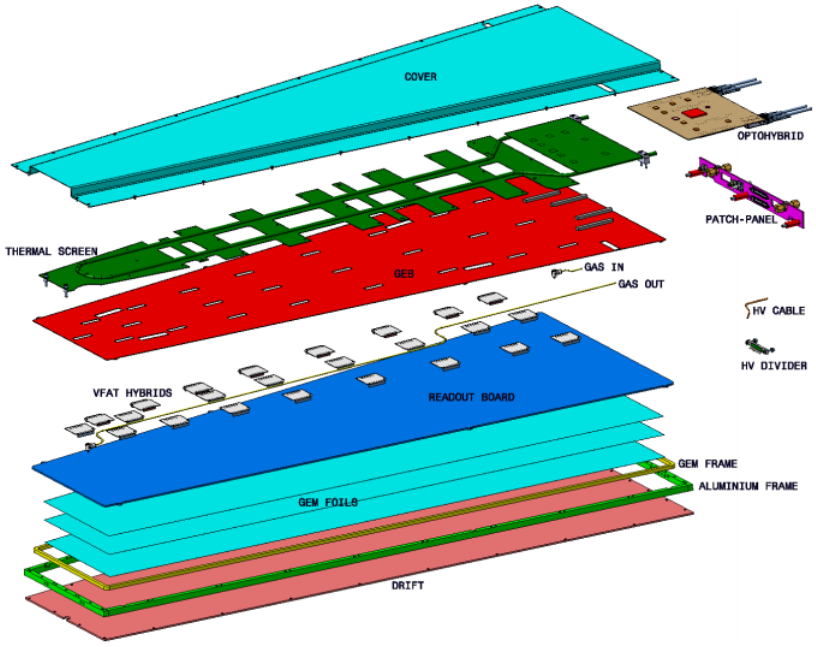

Figure 2.3: Exploded view of the mechanical design of the detector [6].

2.3.1 The GEM detectors

The GEM detector is a gaseous detector and, as all the gaseous detectors, it requires high electric fields in a gaseous environment. An incident particle on the detector creates electron-ion pairs in the gas. The electrons drift by the action of the electric field to a readout electrodes, where they induce an electrical signal read by the acquisition electronics. Along their drift, the electrons can be accelerated by very high electric fields (> 10 kV/cm) to acquire enough energy to ionize the gas themselves, creating a cascade of electron-ion pairs. This process is called an avalanche.

In the triple-GEM detectors, the electrons pass through 3 GEM foils where there is an electric field of more than 50 kV/cm, which produces the avalanche and thus the amplification before reaching the electrodes [6].

The GEM foils

A GEM foil is composed of a 50 μm sheet of dielectric material (kapton), covered on both sides by a 5 μm-thick layer of copper. This sheet is pierced by 70 μm holes spaced out of 140 μm as shown on the left of figure 2.4. A differential voltage is applied between the copper sides, inducing an electric field around the sheet as presented on the right of figure 2.4.

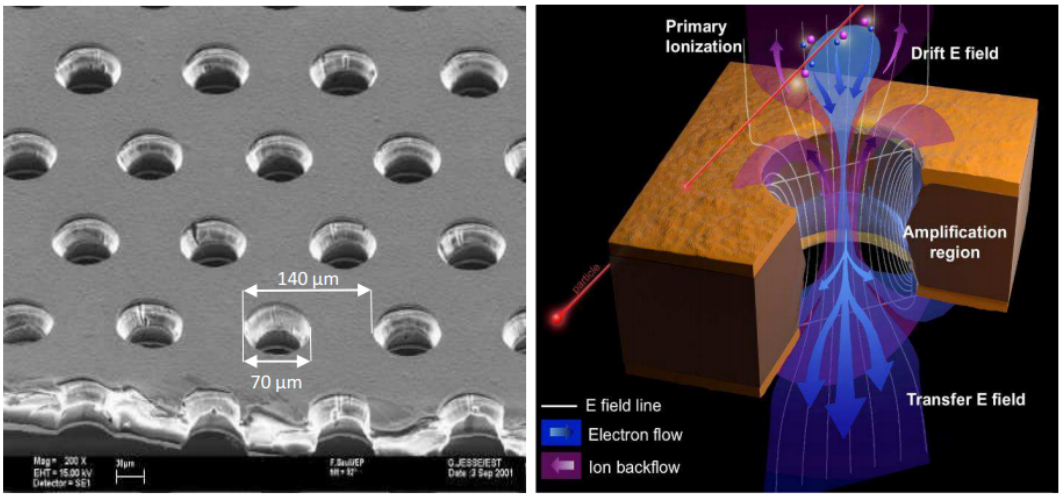

Figure 2.4: GEM foil (left). Schematic view of the electric field lines (white), electron flow (blue), and ion flow (purple) through a hole (right) [6].

As presented on the right of figure 2.4, the electric field lines are focused on the hole center and reach 50 kV/cm. An electron in the gas detector will thus be attracted through the holes. Once in the hole, it will produce a cascade reaction due to the high electric field. Typically, each GEM foil is multiplying the number of electrons by 20, leading to a total gain of 8000 for the triple-GEM [6].

The Readout Board

After the amplification by the triple-GEM, the charges are drifted to the electrode. Figure 2.5 shows the different layers of a triple-GEM detector and the cascade principle induced by a passing particle.

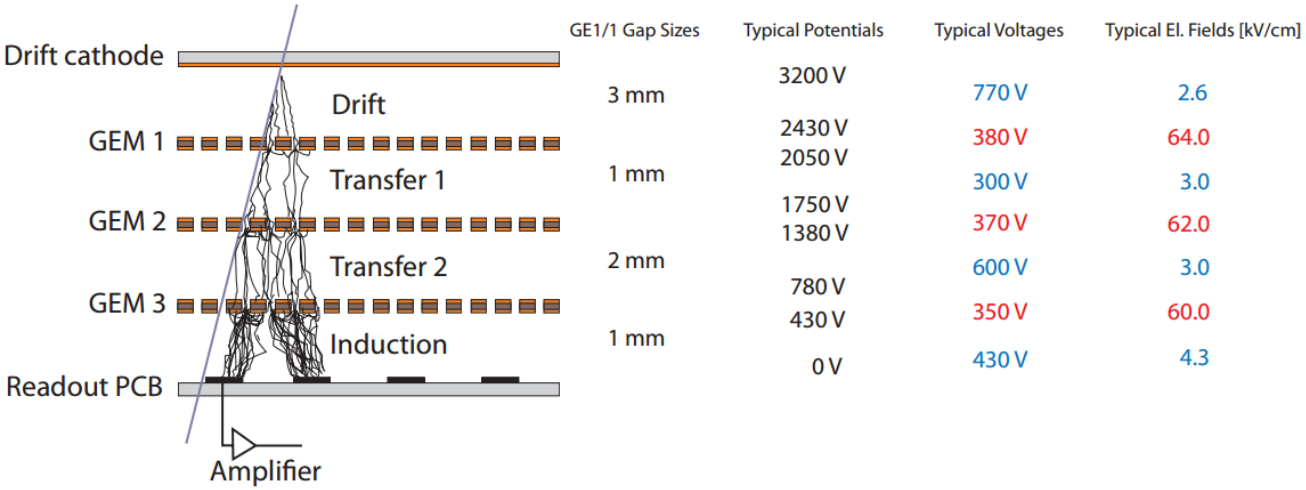

Figure 2.5: Principle of operation of a triple-GEM detector. The spacing between the layers along with the voltages are also presented [6].

As it can be observed on figure 2.5, the readout electrode is divided in strips. In total, the readout board is divided in 384 strips along its width and in 8 sectors along its length. This division ensures that the detectors reach the desired spatial resolution. Indeed, each detector covers 10^o or 0.1745 rad, which means that each channel covers 454 μrad.

The tracks are then gathered in groups of 128 and plugged into a male connector on the other side of the board. The 384 strips are then divided in 3 sections, leading to a final division of the board of $3 \times 8 = 24$ sections. Figure 2.6 present both sides of the readout board.

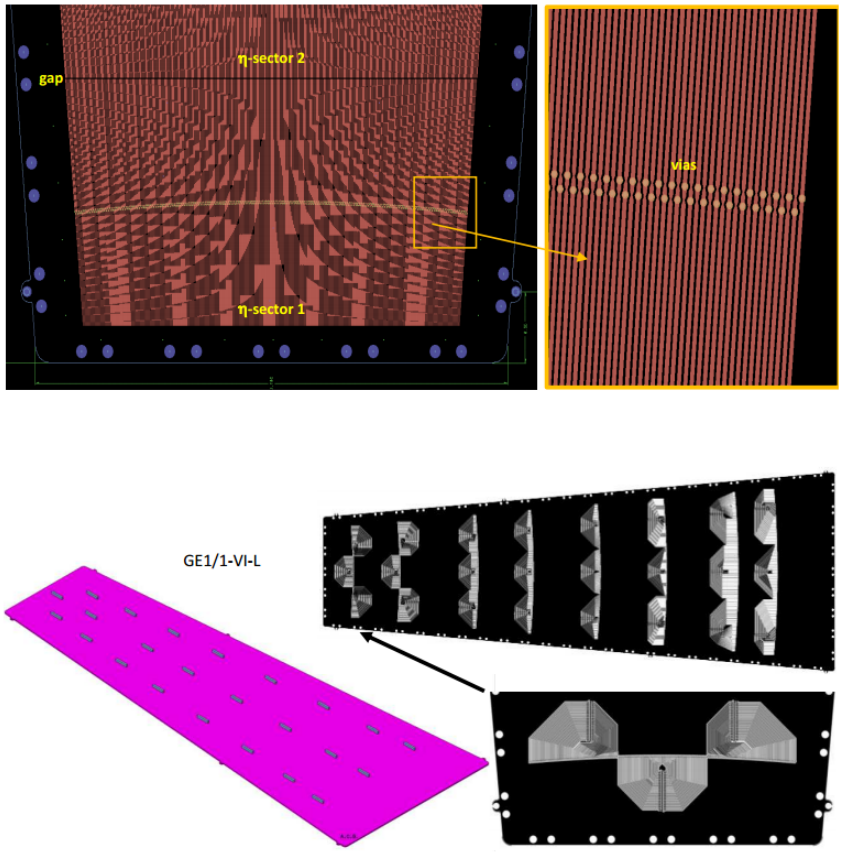

Figure 2.6: The readout board.
Top: GEM side of the readout board. Left: two sectors of the readout board, the hyperbolic geometric pattern is an artifact of the display on a screen. Right: zoom in one of a sector, the strips are visible. Bottom: Other side of the readout board. Left: the 24 male connectors. Right: the 384 strips of each sector grouped by 128. [6]

2.3.2 The GEM Electronic Board (GEB)

The GEB comes on the top of the readout board. It has been designed to support the acquisition electronics, supply it and transmit the produced data. It also has the role of isolating the detector from the noise induced by the electronics. The GEB, presented in red on the top of figure 2.7, is also divided in 24 sectors. Each sector has its own male connector and a hole that lets pass the connector of the detector. A VFAT, which is the first element of the acquisition electronics, is placed on each connectors pair of a sector to send the data from the detector to the rest of the acquisition electronics via the GEB. The disposition of the VFATs is presented on the bottom of figure 2.7. The next chapter will present all that acquisition electronics in details.

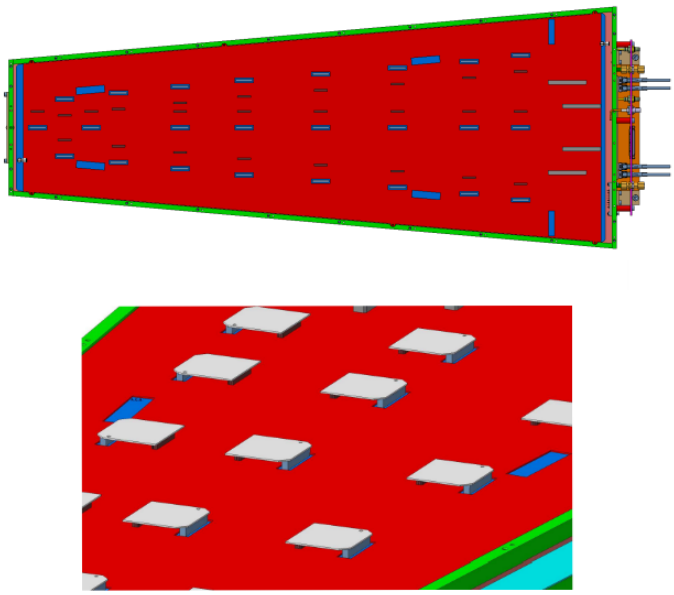

Figure 2.7: The GEM Board
Top: the GEM Board (Red) placed on the top of the readout board (Blue). Bottom: VFAT connection to the GEB and the readout board [6].

Chapter 3

The GE1/1 Acquisition Electronics

Until now, only the physical principles of the detector (transforming a passing particle into an electrical signal) have been introduced. However this electrical signal on the detector strips needs to be measured, processed and transmitted by the system of data acquisition (DAQ). Since this DAQ system is the only way through which the user could observe a particle, it is therefore a key point of the project development. This system is still in R&D, and this master thesis a part of it.

This chapter is dedicated to the presentation of this data acquisition system. First, a general description of the system will be made. Then, each part will be detailed following a bottom-up approach, namely from the electrical signal on the tracks to the user.

3.1 General presentation

A general diagram of the acquisition electronics is presented on figure 3.1.

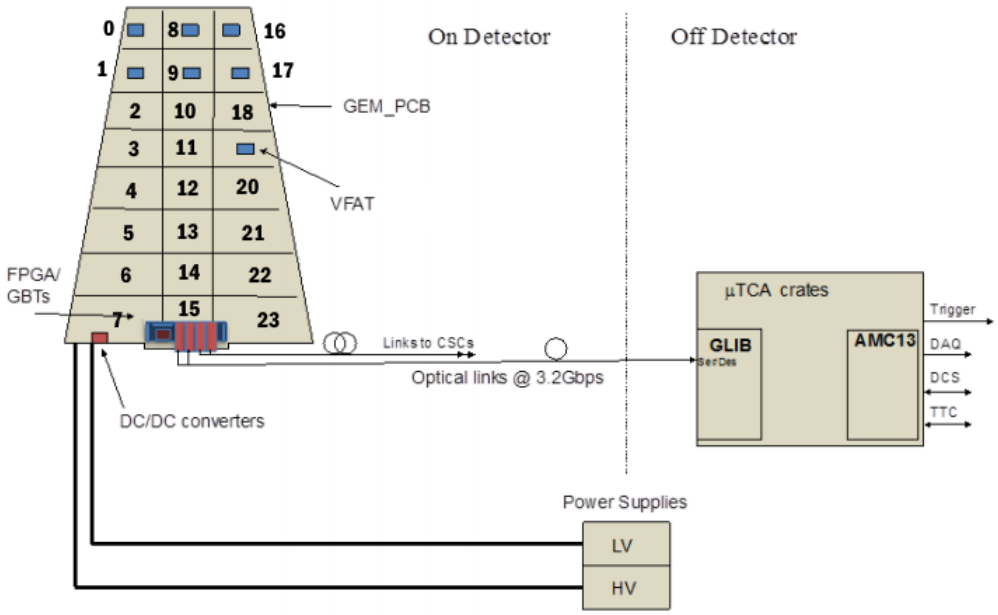

Figure 3.1: Block Diagram of the GE1/1 Acquisition Electronic [7].

The GEB can be easily identified by its trapezoid form. As already explained, the GEB is divided in 8x3 sections, each one has a "position number", as presented on figure 3.1, to be identified. Each section is connected by 128 channels to the detector via a front-end electronics called the VFAT chip.

The VFAT is an ASIC containing 128 channels, each made of a preamplifier, a comparator and a monostable. They produce two signals. The first one is a trigger signal, used to produce the LV1 trigger and sent at the CMS frequency (40MHz). It contains low granularity data, which notifies that a hit has been detected. The second one, the tracking data, is sent only if the hit has been judged to be relevant. It contains all the data produced by the detector, including the high granularity measurements.

The 24 VFATs are then connected via the GEB to the Opto-Hybrid (OH), which is responsible of ensuring the quality of the signal, applying some first level signal processing, and sending the data out of the detector via a bidirectional optical fibre to the off detector electronics.

The transfer of the data between the VFAT and the Opto-Hybrid is done via 2 separates paths. These 2 paths are presented on figure 3.4. The first one, dedicated to the trigger data, is uni-directional with a bandwidth of 320 Mbps. The second one, also uni-directional, sends the tracking data.

3.2 The VFAT chip

The VFAT chip has been originally designed to be used in the TOTEM experiment [9]. It is built in a $0.25\mu m$ CMOS technology and is a synchronous chip working with the LHC master clock at 40 MHz [3]. A block diagram of the VFAT is presented on figure 3.2.

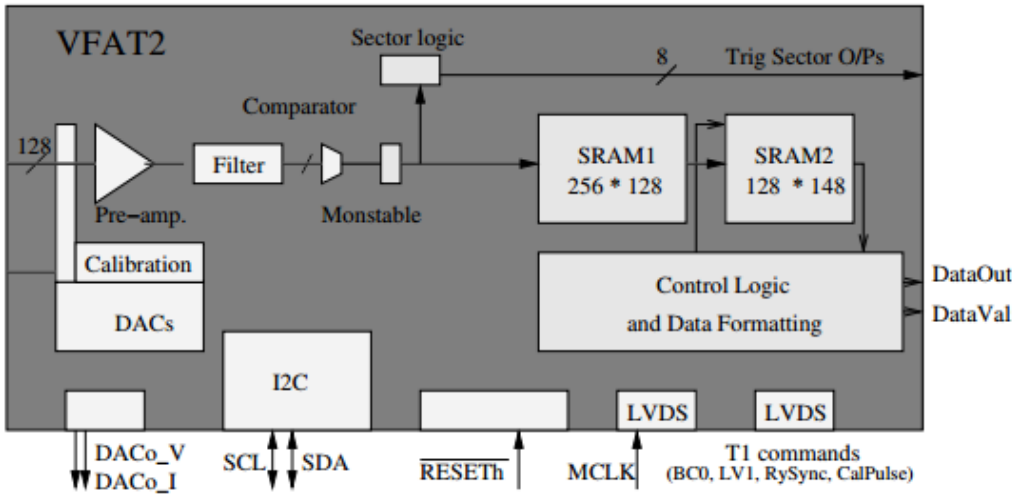

Figure 3.2: Block diagram of the VFAT chip [3].

From the detector, the VFAT is connected to the 128 strips of a sector. Each channel is read at 40 MHz, decomposing the input signals in events. Each event on a channel is then processed through a pre-amplifier and a filter followed by a comparator. The comparator compares the input value with a programmable value, the threshold. This threshold is set by the difference between two 8-bit registers,

called threshold1 (VT1) and threshold2 (VT2).

$$Threshold = VT2 - VT1 \tag{3.1}$$

The use of two thresholds is to ensure a higher flexibility to the VFAT, which can thus work with positive or negative pulses. The triple-GEM detectors produce negative pulse, and the threshold1 (VT1) will thus be used to fix the threshold while the threshold2 (VT2) will be set to 0. If the signal is smaller than the threshold, the comparator produces a logic 1. Such an event is called a "passing event". Figure 3.3 gives an example of a passing event with a negative pulse and a negative threshold.

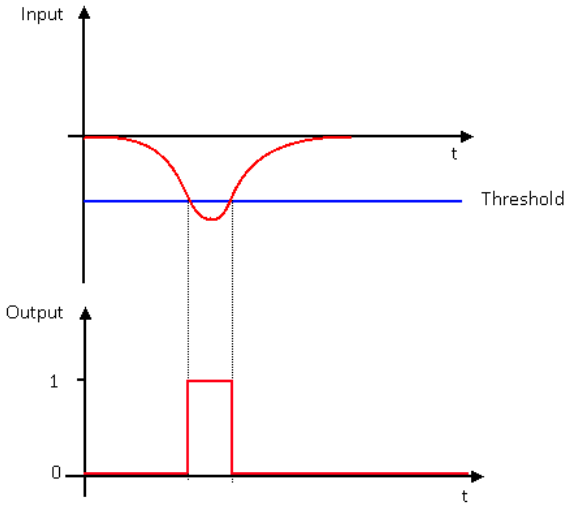

Figure 3.3: Behaviour of the negative threshold comparator

The logic 1 is then kept up for 1 clock cycle by a monostable. If the signal is smaller than the threshold, a logic 0 is produced. This is done in parallel for the 128 channels at 40 MHz. The results are stored in the first of two SRAM memories. As already discussed, the data are then sent out in two different ways: the trigger, that quickly detects a hit, and the tracking data, that holds all the information. These signals are sent to the Opto-Hybrid, following two separate paths. The Opto-Hybrid sends to the VFAT the clock (40 MHz), a reset signal and some command signals. These command signals are quickly explained before a detailed explanation of the tracking and trigger generation.

3.2.1 VFAT commands

Two types of command are sent to the VFAT. The T1 commands, that are the controls of the VFAT during its operating time, and the control signal, used to set the different registers of the VFAT.

The T1 commands

The T1 signal is an encoded signal that contains 4 commands synchronous to the master clock. They are sent via a LVDS (Low Voltage Differential Signaling) protocol to ensure a high speed communication. The 4 commands are: bunch crossing zero identifier (BC0), the level 1 trigger acceptance "LV1A", a synchronous reset "ReSynch" and a calibration timing pulse "CalPulse".

Control signal

All the features of a VFAT are controlled by setting registers. Some examples of important registers that will be used are the 4 8-bits control registers, which globally controls the VFAT, or the 128 8-bits channel registers, which controls each channel separately. These registers are set by the control signals sent by the Opto-Hybrid via a I^2C protocol communication.

3.2.2 Trigger

The generation of the trigger signal takes place before the storage in the SRAM1, directly after the monostable. The 128 channels are grouped together to form sectors. The number of sectors can be chosen between 1, 2, 4 and 8. The trigger signal is then created by using a fast OR on all the channels of a sector. This signal is also called the "s-bit". At each collision, a maximum of 8 s-bits are thus generated, leading to a maximum data rate of 320 Mbps, that justifies the bandwidth of the s-bit path in figure 3.4. If the event is judged to be relevant by the CMS LV1 trigger, the VFAT will receive the LV1A signal sent via the T1 command.

3.2.3 Tracking

Upon receiving the LV1A signal, the corresponding data are transferred from the SRAM1 to the SRAM2. In order to find the data in the SRAM1, the constant delay between the storage in the SRAM1 and the reception of the corresponding LV1A signal is determined and stored in a register. This delay can then be used to find the position of the data in the SRAM1 for every LV1A arriving to the VFAT. Since the delay is not expected to exceed $6.4\mu s$ (corresponding to 256 clock cycles), the SRAM1 is sized to 256×128.

The SRAM2 is sized to 128×148 in order to store 128 triggered data plus headers. Two headers are added to the data, the Bunch Crossing Number (BCN) and the Event Number (EN). The BCN is a 12 bit header generated by a counter that increments every clock cycle. The EN is a 8 bit header also generated by a counter, which increments for every LV1 signal. Both counters are cyclic, and are reset by receiving a BC0 signal via the T1 Command [3].

As soon as data are stored in the SRAM2, the read cycle begin. The Data Formatting block adds a third header, the chip number (16 bit), and streams out the data to the Opto-Hybrid. The chip number is the ID of the VFAT and used to keep track of which VFAT of the detector has produced the data.

3.2.4 Calibration module

The last module of the VFAT is special since it is not used during the data acquisition, but only for the test and the calibration of the VFAT. The Calibration module is used to send calibration pulses (VCal) at the entry of the pre-amplifier as if it was a signal coming from the detectors themselves. Each channel can choose to listen either to the calibration pulse or to the detector. Since there is only one calibration module for the VFAT, not too many channels can listen to the module at the same time, otherwise the Calibration Module could not be powerful enough to produce the calibration pulse for all the connected channels.

3.3 The Opto-Hybrid (OH)

The Opto-Hybrid will ensure the communication between the VFAT to the off-detector electronics. It has to compress and synchronize the data from the 24 VFATs, send them via the optical fiber and ensure the transmission of all the command signal to the VFAT such as the master clock, the reset or the LV1A signal. The Opto-hybrid is placed on the large side of the GEB, as presented on figure 3.4. On this figure, the double path from a VFAT to the opto-hybrid can also be observed.

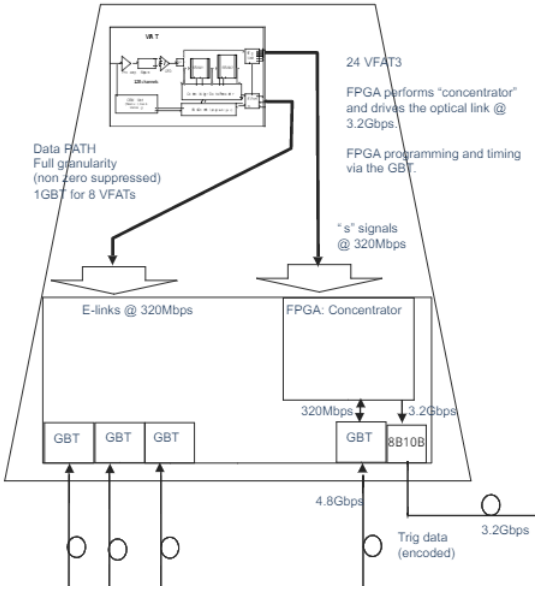

Figure 3.4: Block diagram representing the two paths of data [6].

The Opto-Hyrbrid is equipped with a FPGA, four GigaBit Transceiver (GBT) modules and one 8b/10b module. The FPGA synchronizes the trigger data coming from the 24 VFATs and compresses them (e.g. a zero suppression algorithm). The GBT, combined with a versatile link, forms a bidirectional communication by optic fiber developed by CERN. They offer a low energy communication and a high resistance to the radiation, about 400 Mrad, far superior to the radiation constraint for the GE1/1 project (100 krad). Three GBTs are used to transmit the tracking data out of the detector to the off-detector electronics. The last one is used to transmit the trigger data, also to the off-detector electronics. The 8b/10b module transmits the trigger information to the CSCs detectors. Figure 3.5 is a picture of the acquisition electronic presented until now. The GEB, with the 24 VFATs connected, can be observed just as the opto-hybrid on the bottom of the picture.

Figure 3.5: Picture of the GEB with the VFATs and the Opto-Hybrid.

3.4 The Gigabit Link Interface Board (GLIB)

The GLIB is the part of the off-detector acquisition electronics situated outside of CMS. In CMS, the GLIB board will be hosted in a μTCA crate [18]. It is intended to control, trigger and acuire the data from the Opto-hybrids. It is based on a Virtex-6 FPGA, connected to the Opto-hybrids via GBT links and to a PC with an ethernet port [14].

To end the chapter, figure 3.6 clarifies the different communication protocols between the user and the VFAT. This data path is the one used to communicate with the VFAT.

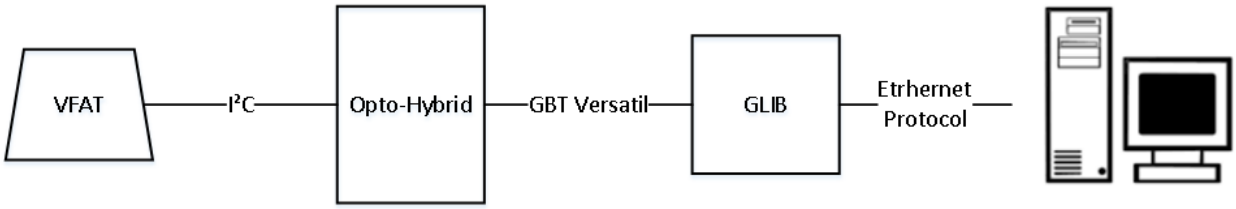

Figure 3.6: Block Diagram of the communication protocols from the VFATs to the user

Chapter 4

The VFAT fonctional tests

In this chapter, two main functional tests of the VFAT are detailed. These functionalities, called the Threshold Scan and the Calibration Pulse Scan (or S-Curve), allow to characterize and to quantify the response of the VFAT chip, globally or channel by channel. The implementation of each functionality has required the development of firmware modules for the Opto-Hybrid and of python scripts to automatize the processes.

4.1 Threshold Scan

As mentioned in section 3.2, a signal detected by the VFAT passes through a comparator. This comparator will output a 1 or 0, depending on the signal amplitude with respect to the programmable comparator threshold. The threshold scan determines the percentage of passing event (1 after the comparator) as a function of the value of the threshold. The scan is made with VT2 set to 0 and by increasing the VT1 from 0 to 255. With respect to equation 3.1, the comparator threshold is thus negative when VT1 is increased. Therefore, only the negative input values are concerned by the threshold scan. The threshold scan can be made for the VFAT in its entirety (scanning all the channels at the same time) or for a single channel. In the first case, the trigger data are used to determine the passing events. In the second case, it is the tracking data of the specific channel that are used to determine the passing events.

A typical shape for a threshold scan is shown in figure 4.1.

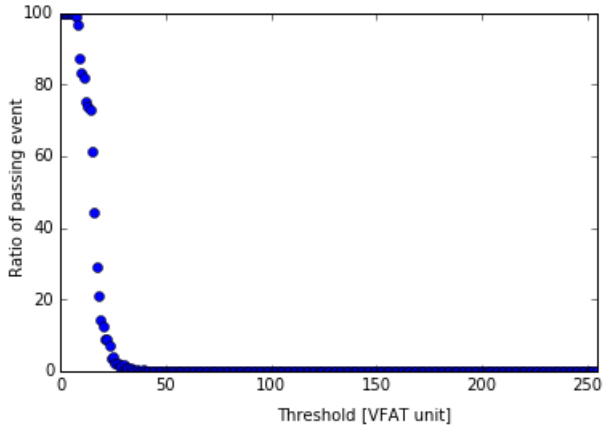

Figure 4.1: Typical shape of a Threshold Scan.

When the threshold is set to 0, all events are considered as passing events, which explains that the curve starts a 100%. By increasing VT1, less and less events are sufficiently negative to be passing events. Typical threshold scans are made by recording 1000 events for every threshold value.

4.2 Calibration Pulse Scan

The calibration pulse scan, or S-Curve, uses the calibration module mentioned in section 3.2.4. For a fixed threshold, the scan will determine the percentage of passing events as a function of the calibration pulse's value. The calibration pulse level (VCal) is set in a register of 8 bits, and therefore goes from 0 to 255 "VFAT unit". This scan has to be done channel by channel and is thus using the tracking data of the specific channel to determine the number of passing events. A typical shape for a the S-Curve is shown in figure 4.2.

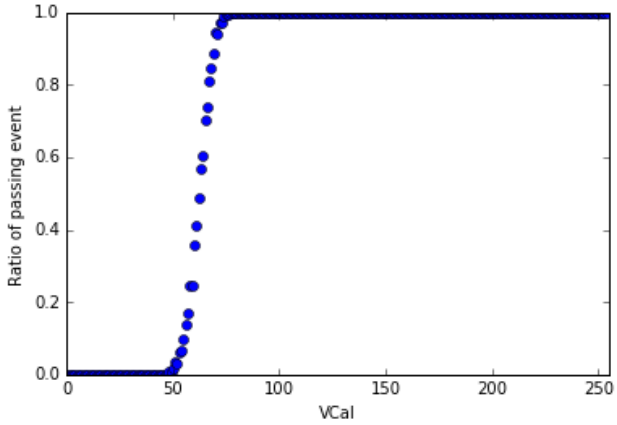

Figure 4.2: Typical "S" shape of a Calibration Pulse Scan.

The S-Curve allows thus to identify at which amplitude (or charge) the input signal is above the threshold. In theory, the S-Curve scan should look like a step, where the step represents the threshold. Indeed, all the calibration pulses with an amplitude below the comparator's threshold should never pass the threshold, and the calibration pulse with an amplitude above this threshold should always be passing events. The value of VCal at the step is called the "detection level".

However, as shown on figure 4.2, the noise degrades the curve and gives it a "S" shape. The value of the detection level is no longer well defined and is located at the point where the S-Curve is equal to 0.5. The spread of the S-Curve is therefore an indicator of the noise on the channel. An illustration of the degradation by the noise is shown figure 4.3.

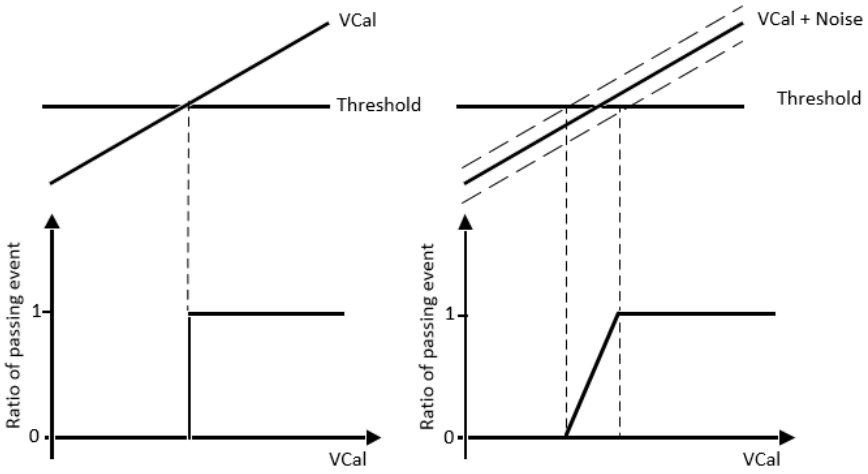

Figure 4.3: Degradation of the calibration pulse scan with the noise.

4.3 The cumulative distribution function Fit

In order to precisely extract the results from them, the S-Curves can be fitted with the cumulative distribution function (CDF) of the standard normal distribution:

$$CDF = \frac{1}{2}(1 + erf(\frac{x-\mu}{\sigma\sqrt{2}})) \tag{4.1}$$

where erf is the error function. The shape of the CDF and the effects of its parameters are shown on figure 4.4.

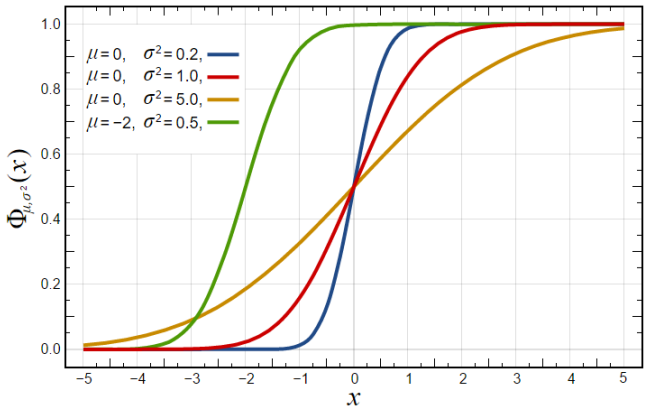

Figure 4.4: Cumulative distribution function (CDF) of the standard normal distribution.

When the cumulative distribution function is fitted on the S-Curve, two parameters are adjusted. First, the mean, that will translate the intercept of the CDF to fit with the VCal value when the S-Curve equals 0.5. It then represents the detection level of the S-Curve.

Second, the standard deviation, that will modify the slope of the CDF. The standard deviation is then related to the noise: when it is equal to 0, the CDF is a step (no noise) and its increase reduces the slope (increase of the noise). These parameters allow to quantitatively define the S-Curves.

4.4 TrimDAC

So far, the threshold of the comparator is fixed in a global register and is the same for all channels of a VFAT chip. As it can be expected, all the channels do not behave in the exact same way and a unique threshold leads to different detection levels for each channel. The trimDAC functionality allows to tune the threshold for each channel. It is coded on 5 bits in the channel register and thus takes a value between 0 and 31.

Since the trimDAC functionality has never been used before, a characterization of its effect must be done.

4.4.1 Characterization of the trimDAC

When the trimDAC is increased, its effects can be observed both on the threshold Scan and on the S-Curve.

Threshold SCan

When the trimDAC is increased, the threshold Scan is shifted to the right as shown on figure 4.5.

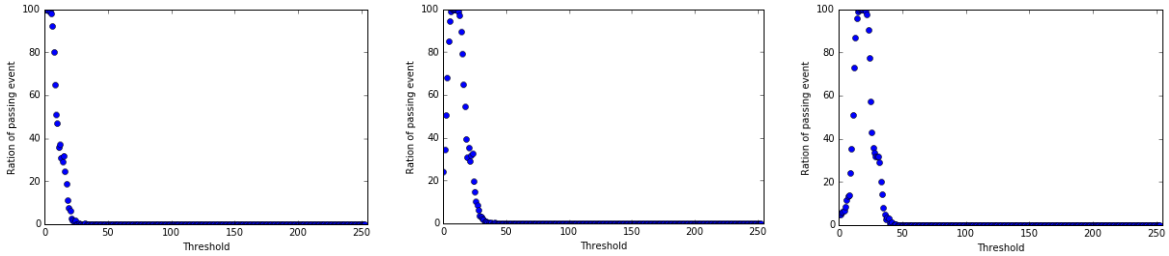

(a) TrimDAC = 0 (b) TrimDAC = 16 (c) TrimDAC = 31

Figure 4.5: Effect of the trimDAC on a threshold scan.

It is important to note that it is a shift and not a widening of the curve: the number of "VFAT Unit" needed to go from 100% to 0% is constant in the three cases (around 23 VFAT units for figure 4.5). Due to the shift, the positive input values appear now on the left of the figure.

S-Curve

When the trimDAC is increased, the S-Curve is shifted to the left, as seen on figure 4.6.

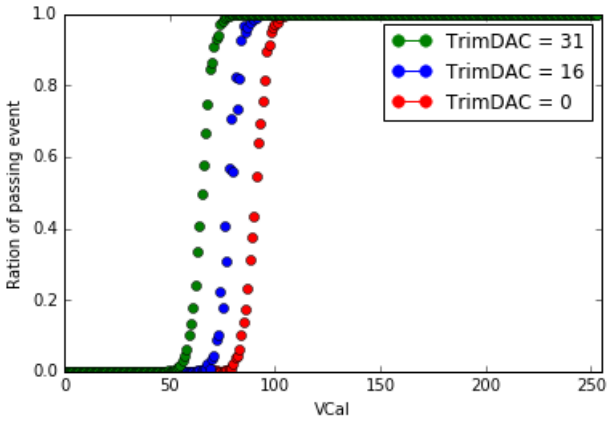

Figure 4.6: Effect of the trimDAC on a S-Curve

This behaviour seems to indicate that the increase of the trimDAC improves the channel sensitivity: the detection level will be lower for higher trimDAC values.

From these measurements, the behaviour of the trimDAC can be summarised by adding a term to the threshold of the comparator by channel. It can now be computed as:

$$Threshold_{channel} = VT2 - VT1 + \alpha \cdot trimDAC_{channel} \tag{4.2}$$

with α a conversion factor. This explains the positive value for a VT1 and a VT2 set to 0 on the threshold scan. It also explains the increase in the channel sensitivity since the threshold for that channel will be closer to 0. Graphically, this term tends to rise the threshold level on figure 3.3. To keep the same distance with the noise level, and thus maintain the efficiency of the system, VT1 needs to be increased.

Once these functionalities were implemented in firmware and software, the full VFAT calibration procedure could have been developed. The next chapter will present this procedure in details.

Chapter 5

The VFATs Calibration Procedure

When the VFATs are operating in CMS, they should work at their best settings. First, the threshold should be as small as possible. Indeed, the value of the threshold is directly proportional to the detection efficiency of the system: reducing the threshold increases the efficiency. However, the threshold should be kept high enough with respect to the noise. As seen in section 2.2, a detection efficiency of 97% is the objective for the project, it corresponds to a typical VT1 value of 25. However, as seen in chapter 4, adjusting the trimDAC values may require a higher VT1 value to maintain the same detection efficiency.

Secondly, all channels of a single VFAT should, as much as possible, behave in the same way to provide a uniform response on the VFAT chip. It means that all channels should have the same output for the same electrical signal at the input, or stated differently, the detection level for all the channels should be the same.

A well defined behaviour means that the characteristics of the VFAT should be known, e.g the value of the relevant parameters, the value of the threshold and of the trimDAC, or the value of defective channels - dead channels or abnormally noisy channels.

A procedure is then necessary to correctly calibrate the VFAT. A python script has been developed in order to automate this procedure of calibration on a complete GEB (equipped with the 24 VFATs). This calibration procedure represents the first part of the master thesis. It is realised with the VFATs connected to the detector, but with the detector shut down so that the only input signal is the noise. The next sections will detail the step of the script and its results.

5.1 The calibration script

The script begins with some preliminary tests. It detects the presence of the GLIB and the presence of the Opto-Hybrid, test their registers, scans the GEB to detect the position where VFATs are connected and their corresponding IDs, tests the I2C communication with each VFAT and tests the acquisition of tracking data. Then, the script will automatically run the calibration procedure for all the connected VFATs detected during the preliminary tests.

The first step of the calibration procedure is to set the trimDAC of the channels to their median value, 16, and to realise a threshold scan. Since the detector is not powered, only the noise generates signals on the VFAT channels. The threshold is thus set to the its minimal value that ignores all the noise - in other words, the value of the threshold from which their is no more passing events. By doing this manipulation, the script set a valid threshold anticipating the trimDAC tuning.

Secondly, 3 S-Curves are realized for each channel. The first S-Curve is done with the trimDAC set to 16, and will be used to characterize the behaviour of the VFAT before any modification by the script. The two other S-Curves are done respectively with a trimDAC of 0 and 31. From these S-Curves only the detection level is saved to be used in the next step.

Once all the channels have been scanned, the average detection levels are determined for the trimDAC 0 and the trimDAC 31. From these two averages, the detection level wanted for all channels

of the VFAT is computed. This methodology allows to find the average detection level that could be most easily reached by as much channels as possible.

After that, the script sets the trimDAC of each channel so that its detection level is as close as possible of the average detection level determined above. This procedure is called the "trimDAC routine". Once all channels are set with the optimum trimDAC, a second threshold scan is done to be compared with the first one. Figure 5.1 presents a flow chart of the script.

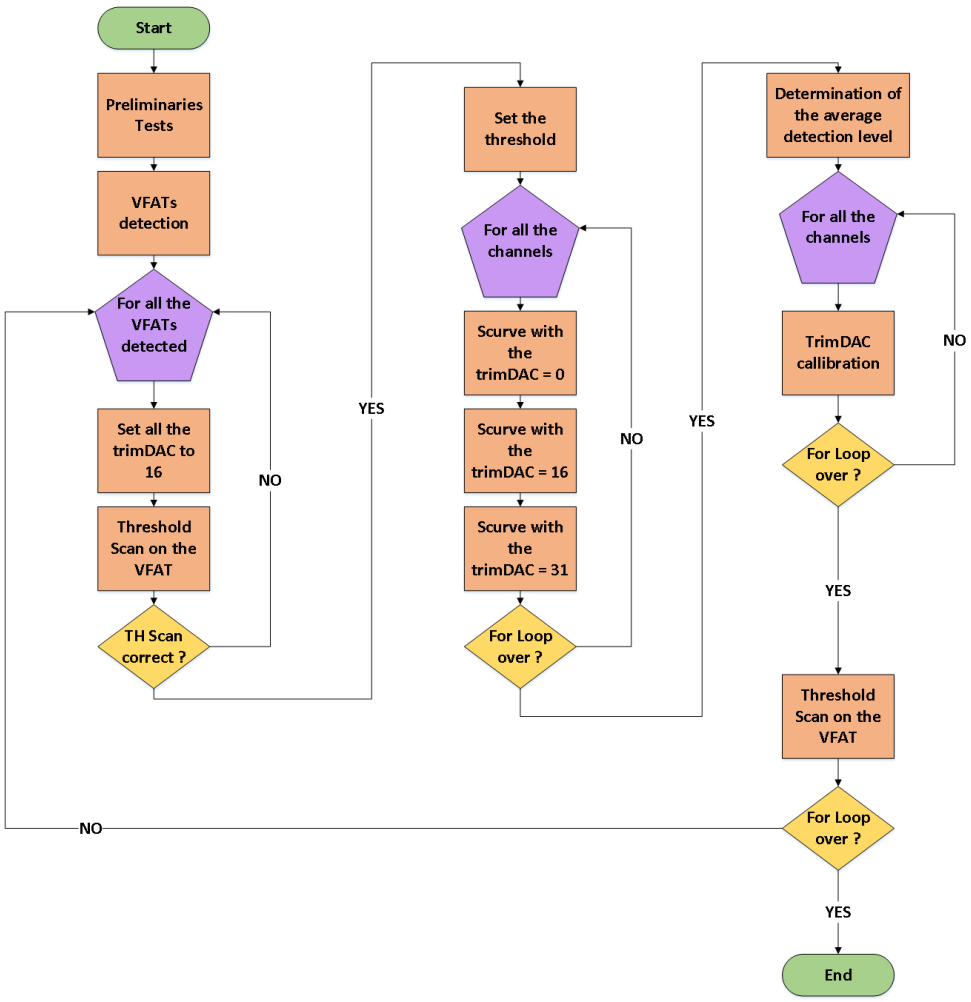

Figure 5.1: Flow Chart of the python script

At the end of the script, all the VFATs on the GEB are thus set with a threshold value where the noise level is below 0.1% and when the detection efficiency is expected to be higher than 95%, and all the channels of each VFAT have the same behaviour. The script produces 5 text files containing all the results for each VFAT. A second python code ("*read_and_plot.py*") reads these files and produces graphical results. The next sections will present typical results for a correctly operating VFAT.

5.2 The results of the calibration procedure

The first results are the two threshold scans, as shown in figure 5.2, along with the value of the threshold set for the calibration procedure. These results are a first indicator of the noise level on the VFAT. This plot also allows to verify if the threshold is still correct after the calibration procedure.

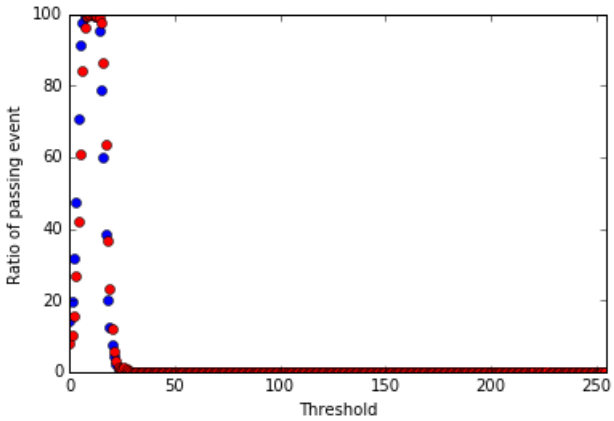

Figure 5.2: Threshold scans before (blue) and after (red) the calibration procedure.

Secondly, the code will output several graphics to observe the alignment of the channel detection level. First, it generates as 2-D color maps, the S-Curves for each channel as a function of the VCal amplitude, before and after the calibration procedure, as seen on figure 5.3.

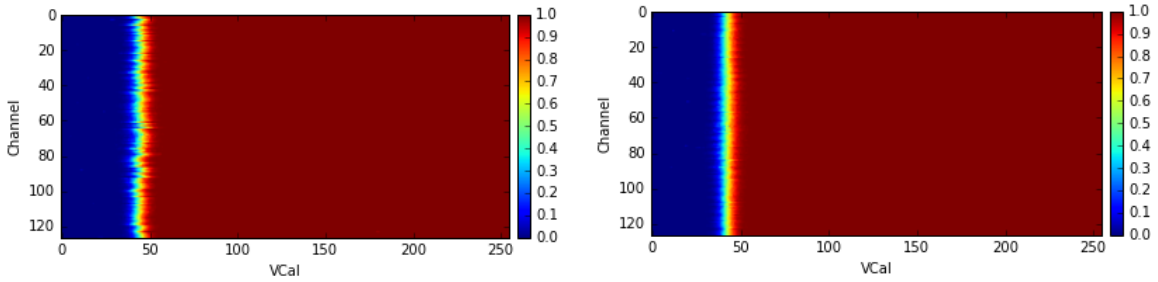

(a) Before (b) After

Figure 5.3: S-Curves before and after the calibration procedure.

These graphs allow to observe the channels miss-alignment before the script and to check if the channels are correctly aligned after the procedure. They are plotted along with the variance of the detection level. For the example shown on figure 5.3, the variance has been reduced from 1.77 to 0. A second plot characterizing the alignment of the channels is the histogram of the detection level (the 0.5 point) for the S-Curves done with the trimDAC set to 0 and 31, as well as for the S-Curves after the calibration procedure. It is shown on figure 5.4.

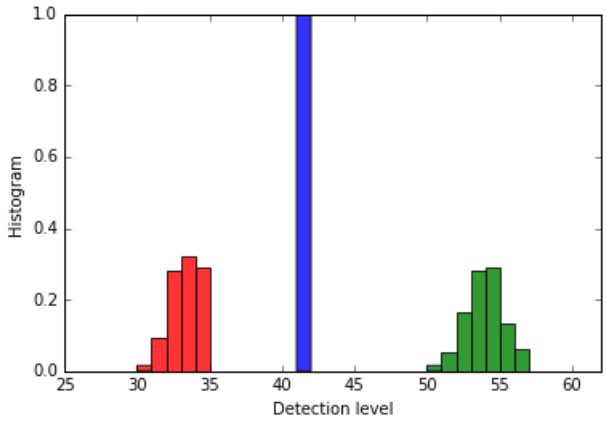

Figure 5.4: Histogram of the detection level for the trimDAC=0 (green), trimDAC=31 (red), and after the calibration procedure (blue).

As expected, the final detection level is the same for all the channels and with a value equal to the mean of the S-Curve's detection levels with the trimDAC set to 0 and 31.

From the results of the script, further information on the VFAT can be extracted. It is presented in the next section.

5.3 Complementary results

The python code "*read_and_plot.py*" producing the graphical results from the text files fit also all the calibrated S-Curves with a cumulative distribution function (see section 4.3). To optimize the fit, the routine focuses only around the step part of the S-Curve. Two parameters are also added to the fit procedure: a parameter for a vertical translation and a parameter for a vertical compression of the CDF. The addition of the two parameters relaxes the fitting on the edge to optimize the fitting of the detection point and of the slope, which are the relevant data that are extracted from the fit.

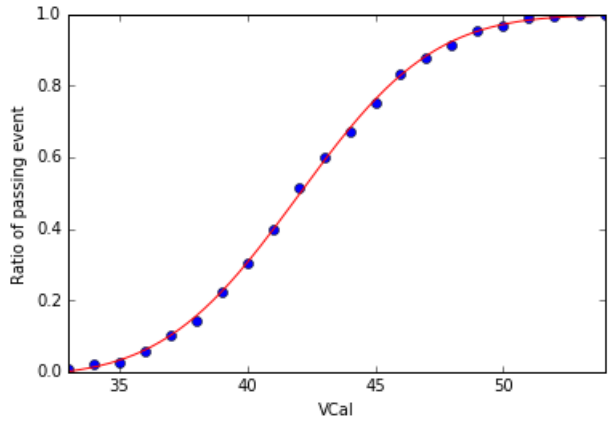

Figure 5.5: Fit of a S-Curve with the CDF.

The mean and the standard deviation are then determined from the fit. The mean is plotted channel by channel as shown on figure 5.6. The standard deviation is graphically presented channel by channel, such as the mean, and also by a histogram, itself fitted by a Gaussian, as shown in figure 5.7.

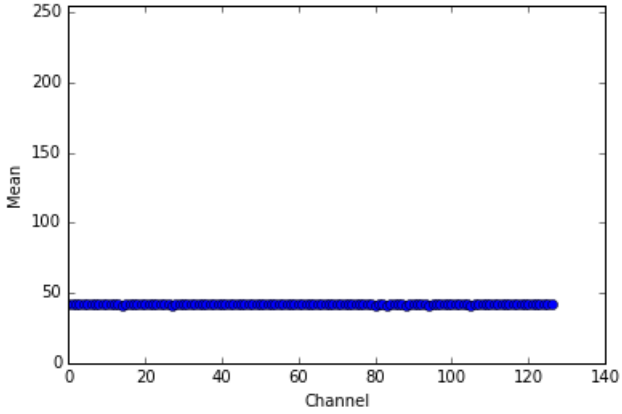

Figure 5.6: Mean of the CDF fitted on the S-Curves.

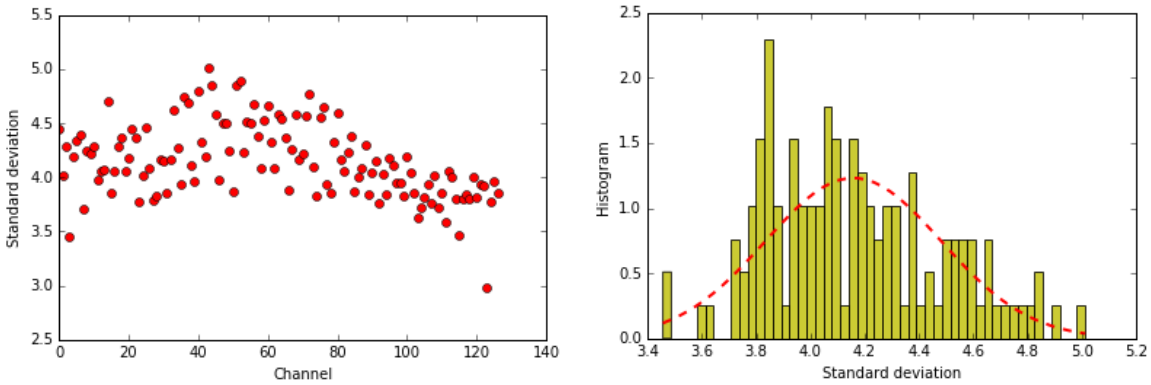

(a) Repartition by channel.

(b) Histogram fitted by a Gaussian.

Figure 5.7: standard deviation of the CDF fitted on the S-Curves.

Finally, the code creates a summary file for each VFATs containing all the VFAT settings and important results:

- The date and time of the scan
- The VFAT ID
- All the settings parameters used for the scan
- The VT1 and VT2

- The median TrimDAC value
- The detection of each channels after the script
- The standard deviation of each channels after the script
- The TrimDAC of each channels after the script

These files are destined to be stored to create a database of the VFATs behaviour.

The information that has been extracted from all the previous results is a detailed representation of each VFAT on the GEB. The calibration procedure proposed in this master thesis has become now the main quality control process of the VFAT production for the GE1/1 project. It is now in used at CERN to test and qualify the 3500 VFATs chips needed for the whole project.

The second part of the master thesis uses this script to collect as much data as possible from the VFATs in a well defined way. These data have been useful to find, understand and solve issues in the acquisition electronic. This part is detailed in the next chapters.

Chapter 6

VFAT Characterization

First of all, a clarification about the measurements presented in this chapter needs to be done: the calibration script has been presented so far in its final form, but it was in constant evolution during the master thesis due to the different observations and the improvement of the system understanding. The present chapter will therefore present the various issues observed during the master thesis with the help of the calibration procedure. Once most of the issues have been solved or understood the correct characterization of the VFAT has become possible.

The scans have been done in two different cases: with the VFATs connected to the detector and with the VFATs not connected to the detector. The first case, which will be detailed in this chapter, is useful to analyse the behaviour of the acquisition electronics with the minimum of external perturbation. The case with the VFATs connected to the detector is detailed in chapter 7.

6.1 Preliminary Threshold Scan

The first step has been to make a simple Threshold scan, with all the trimDAC set to 0, on all the VFATs on one GEB. Figure 6.1 presents the results with the position numbering following the scheme presented on figure 3.1. Two observations can immediately be made: first, the VFATs on the central column seem to suffer from a higher noise which brings the fast falling edge of the curve to values around 50 VFAT units against a few VFAT units for the other columns. Secondly, a few VFATs (on position 13, 20 and 23) present a constant fraction of passing events at 100% up to the maximum threshold value. In the next 2 subsections, these observations are interpreted.

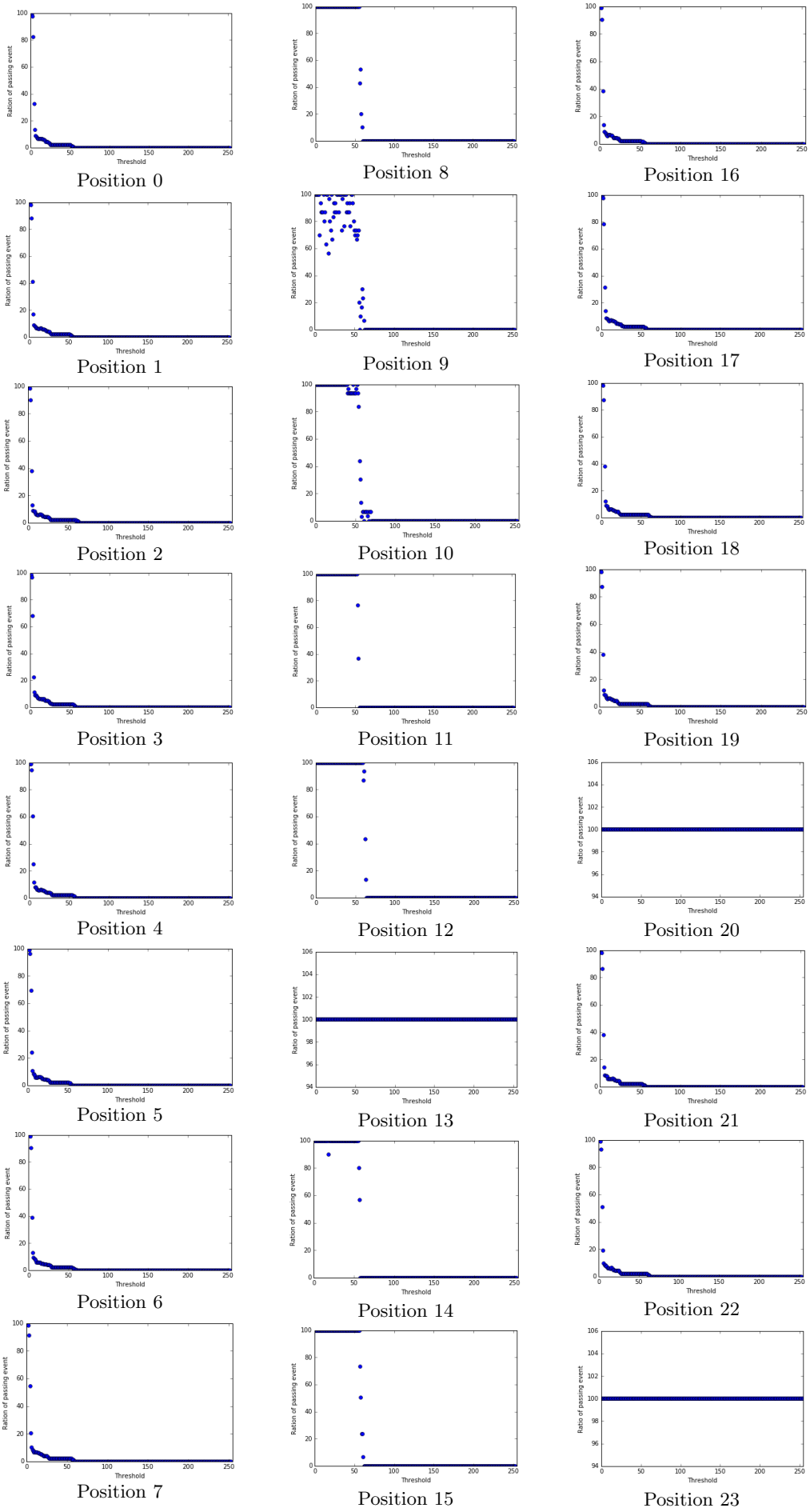

Figure 6.1: Threshold scans on the 24 positions of the GEB.

6.1.1 Central Column dysfunction

The noise observed on the central column VFATs cannot be explained by the thermal noise at the pre-amplifier input. Permuting VFATs does not help, which indicates that the noise does not come from the VFAT itself. The problem is most probably due to a mistake in the GEB design, where some lines have been wrongly routed to the Opto-Hybrid. A patch has been implemented by cutting some pins on the OH and re-soldering small wires, but apparently the fix is not perfect. The GEB design mistake will be corrected in the next version which will be produced in June 2016.

6.1.2 Dead Positions

The second problem was the VFATs on positions 13, 20 and 23, which always return 1. The scan on these positions have been re-done with different VFATs and the results were the same. The problem is thus coming from the position on the GEB and not from the VFATs. In order to check if the problem was redundant over the GEB, the scan has been run at the CERN on a different GEB. There were also some positions returning always 1, but not the same as on the IIHE GEB. The problem is thus technical, as burned connectors or broken wire on the GEB. This is not a problem in itself, just an illustration of the fragility of the GEB.

6.2 The I2C noise

Another undesired behaviour that can be observed on figure 6.1 is the long tail on the threshold scans. A detailed view is shown on figure 6.2 where the fast falling edge is followed by a king of shoulder ending around 50 VFAT units, followed by a long tail at 1% up to 200 VFAT units. The probability that, for each event, the VFAT has 1% chance to send a false passing event is unacceptable. With the frequency of the CMS collisions, 40MHz, that would mean 500kHz of false passing events per VFAT. If the threshold is set beyond the tail to ignore the noise, that would tremendously degrade the efficiency of the detector. It this thus necessary to get rid of it. The full script has thus been launched on the side columns of the GEB to learn more about these tails. The two threshold scans presented on figure 6.2 show the scans for one position with the trimDAC set to 0 (blue) and with the trimDAC set to 16 (red).

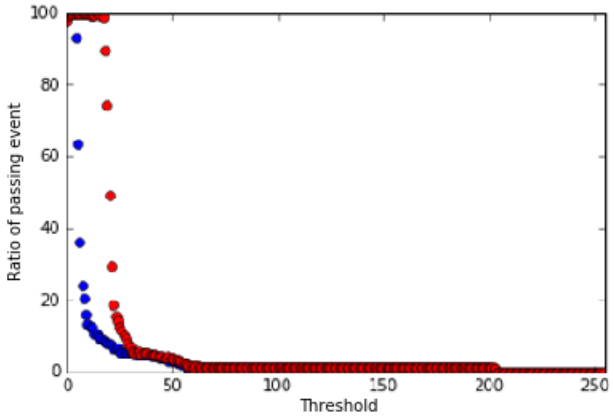

Figure 6.2: Threshold scans with the trimDAC to 0 (blue) and with the trimDAC set to 16 (red).

An interesting observation is that the tail is not shifted when the trimDACs are increased. This observation can be done on all the position scanned. That means that the threshold level of the comparator has no effect on the length of the tail. The measurements are thus degraded after the comparator, either by the VFAT itself or during its transmission trough the acquisition electronic. To better understand the behaviour of the tail, a threshold scan by channel has been done. The result of this scan is presented of figure 6.3 for the VFAT on the position 1.

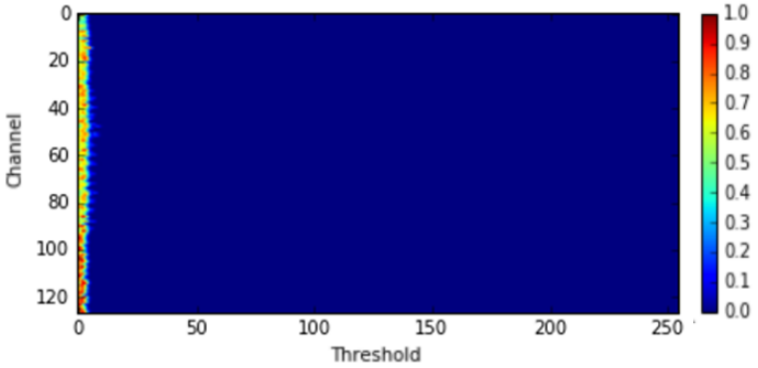

Figure 6.3: Threshold scan by channel for the VFAT on position 1.

On this scan, no tail can be observed, which means that the results coming from the detector are correct, along with the transmission of the tracking data through the electronics. At this point, it is important to remind a property of the threshold scan. As mentioned in section 4.1, different data are used for the threshold scan depending if it is done for the VFAT or by channels. By channels, the tracking data are read, while for the VFAT, only the trigger signal is. The tail is thus coming from a problem in the trigger generation or on the trigger communication line. After investigation on the GEB architecture, it has appeared that the trigger communication lines are parallel with the clock lines of the I^2C communication. The tails were thus coming from a cross talk between the lines. A modified version of the firmware on the Opto-Hybrid has been implemented. In this new version, the I^2C clock is shut down when the communication is unused. When the calibration script is ran with the new firmware version, and by looking carefully not to use the I^2C communication during the data acquisition, the tail completely disappears from the threshold scan as shown on figure 6.4. Ideally, the use of the I^2C communication should be possible during the data acquisition. Hardware specialists are thus working to find a way to isolate the two lines and avoid this cross talk for the next GEB generation.

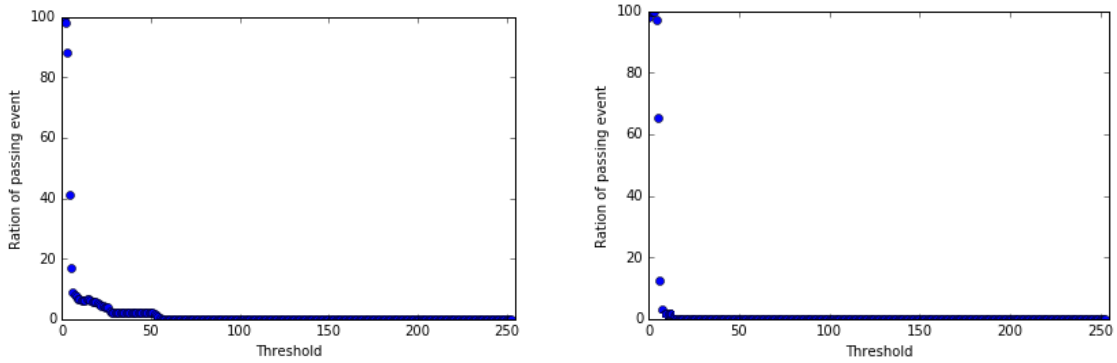

(a) Old firmware

(b) New firmware

Figure 6.4: Difference of the firmeware version on the threshold scans for the same VFAT on the same position.

6.3 Voltage Regulator noise

Not shown so far, some VFATs actually produce very noisy measurements even if the I^2C clock interference is solved. Figure 6.5 compares the threshold scan of one of these noisy VFAT with the threshold scan of a typical VFAT for the same position on the GEB.

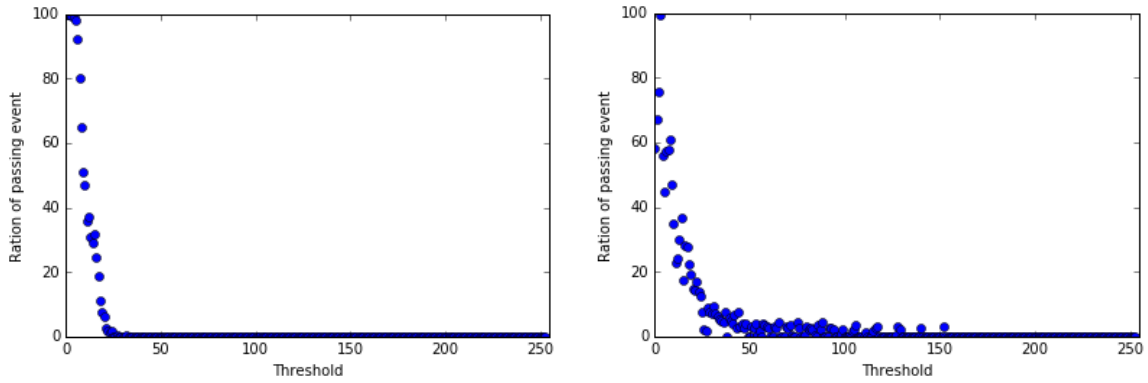

(a) Small Voltage regulator

(b) Big Voltage regulator

Figure 6.5: Threshold scan on the same position for a VFAT with a small regulator and a VFAT with a big regulator.

By taking a look on the physical device, a difference can be observed between the two VFATs as shown on figure 6.6.

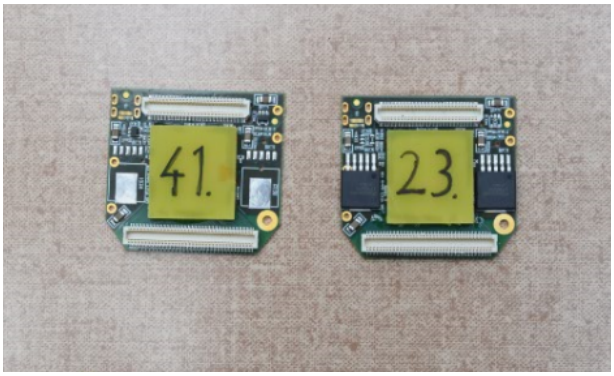

Figure 6.6: Pictures of two VFATs.

The components next to the VFAT chip (in the center of the PCB hybrid) are the voltage regulator blocks. These regulators prevent the voltage to exceed the nominal tension of the VFAT, i.e. 2.5V. Below this voltage, they have no effect on it. As it has been observed on figure 6.6, there are two versions of the voltage regulator on the VFATs: the TP573650 (left) and the LP38501 (right). All the noisy VFATs are equipped with a LP38501 voltage regulator. It seems thus that it is these regulators that produce the noise. To confirm this theory, three threshold scans have been made on a VFAT equipped with a LP38501 regulator. The first one with a voltage of 2.58V, the second one with a voltage of 2.43V, and the third one with a voltage of 2.53V but with the voltage regulator bypassed. The three results are presented on figure 6.7.

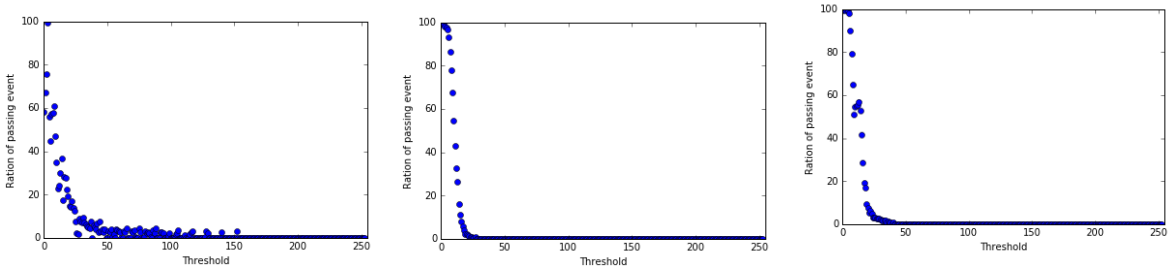

(a) V = 2.58V

(b) V=2.43V

(c) V = 2.53V and regulator bypassed

Figure 6.7: Effect of the LP38501 voltage regulator on the threshold scan depending of its use.

When the regulator is not used, the VFAT suffers from significantly less noise. That confirms the theory that the noise is induced by the LP38501 voltage regulator. Even if they seem not noisy, the same procedure has been applied to the TP573650 voltage regulators. The results are presented on figure 6.8.

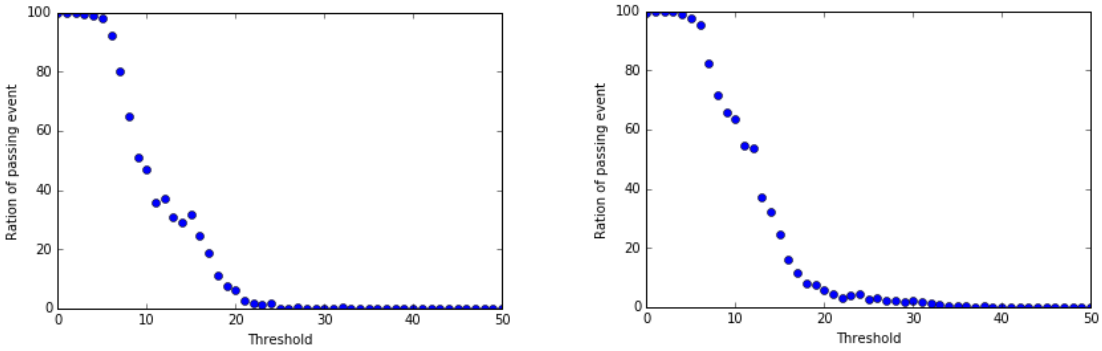

(a) V=2.48V (b) V=2.6V

Figure 6.8: Effect of the TP573650 voltage regulator on the threshold scan depending of its use.

As for the LP38501 regulators, the TP573650 regulators also increase the noise on the VFAT, but to a lesser extend. In all cases, the VFATs with the small regulator should be used. The noise could be reduced by working either at the right voltage without regulator - but it could be dangerous for the VFAT in case of surge, or to work with a voltage slightly smaller than the nominal value of 2.5V - but in that case there is a risk to work with too low voltage. The next section is dedicated to the analysis of the under nominal voltage operation of the VFAT.

6.4 Low voltage operation

Since the VFAT seems to operate correctly with a voltage of 2.45V (lower than the nominal value of 2.5V) which could make the regulator inactive and therefore reduce the noise, the VFAT functionalities at even lower voltages have been tested. The observations are the following: at 2.3V, the VFAT cannot produce powerful enough calibration pulses to rise the S-Curve to one. At 2V, no calibration pulse is powerful enough to produce a passing event on the VFAT. In conclusion, the risk to work at lower voltage and produce wrong measurements is thus too high and the VFAT should be used with a voltage higher than 2.5V to guarantee a tension after the regulator at 2.5V.

6.5 Channels behaviour analysis

Resulting from the previous observations, the measurements have then been focused on the 2 lateral columns, using only VFATs equipped with a TP573650 low-noise regulator and with the updated version of the firmware. Typical thresholds scans and the S-Curve obtained in these conditions are shown on figure 6.9 and 6.10 respectively.

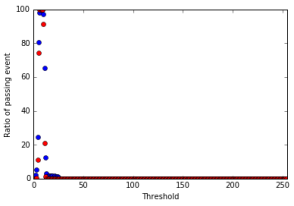

Position 0

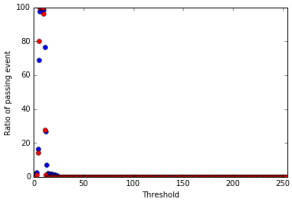

Position 16

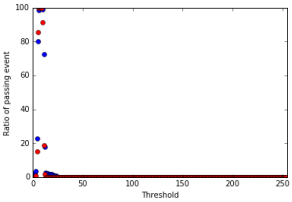

Position 1

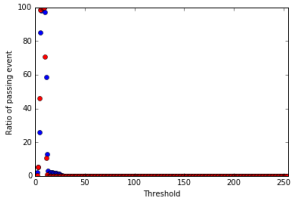

Position 17

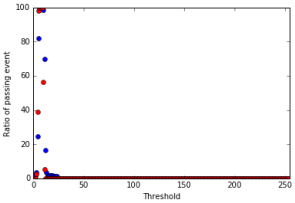

Position 2

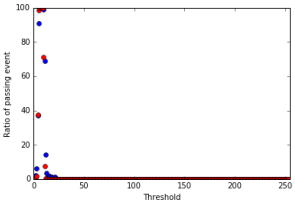

Position 18

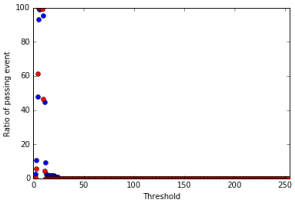

Position 3

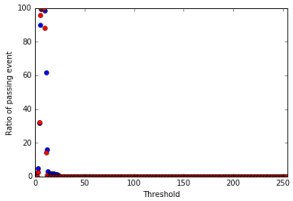

Position 19

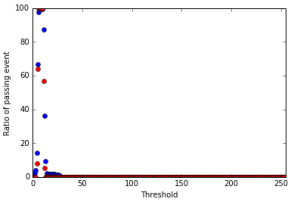

Position 4

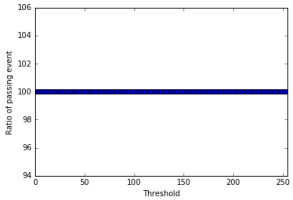

Position 20

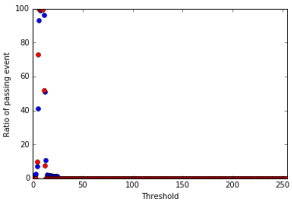

Position 5

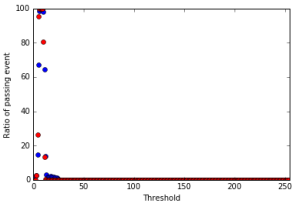

Position 21

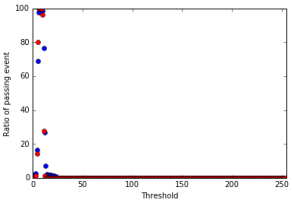

Position 6

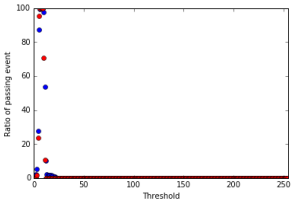

Position 22

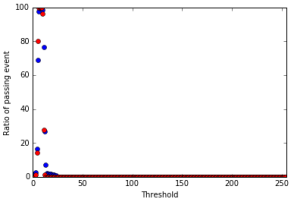

Position 7

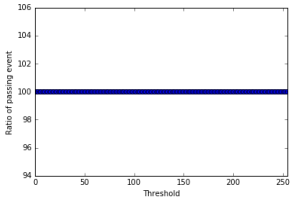

Position 23

Figure 6.9: Threshold scans of the VFATs not connected to the detector.

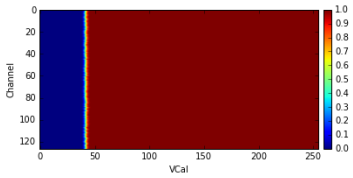

Position 0

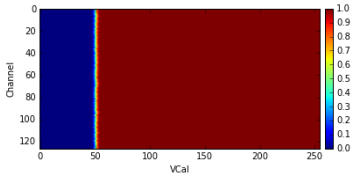

Position 16

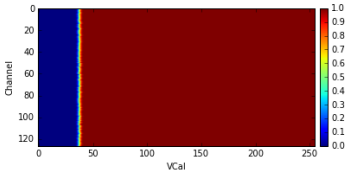

Position 1

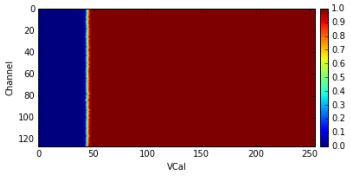

Position 17

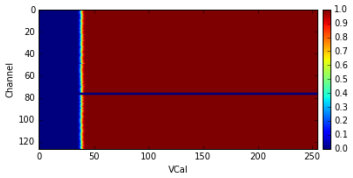

Position 2

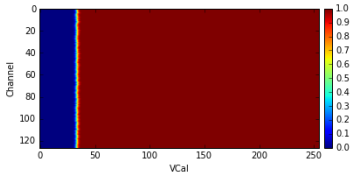

Position 18

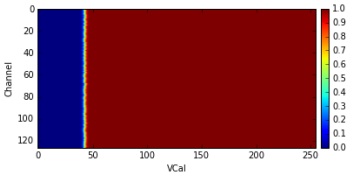

Position 3

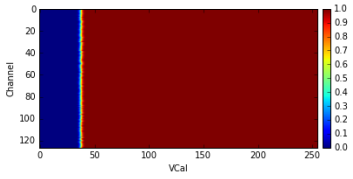

Position 19

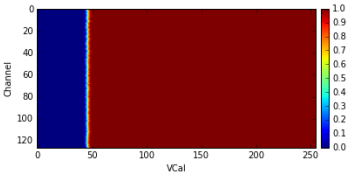

Position 4

DEAD POSITION

Position 20

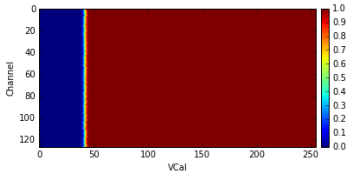

Position 5

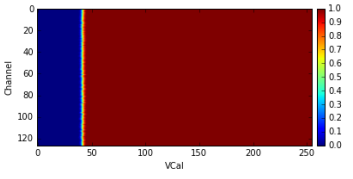

Position 21

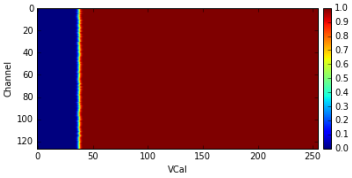

Position 6

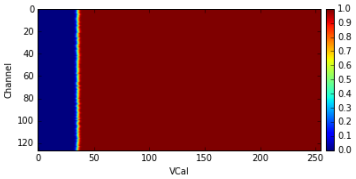

Position 22

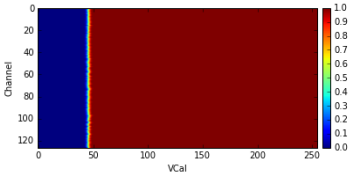

Position 7

DEAD POSITION

Position 23

Figure 6.10: S-Curves of the VFATs not connected to the detector.

As it can be observed on figure 6.9, the tails have completely disappeared with the new version of the firmware. The use of VFATs equipped with TP573650 low-noise regulators allows to obtain small noise levels (less than 25 VFAT Unit on the threshold scans). Only the positions that were at 100% for all the threshold values have not been positively affected by the changes. Regarding the S-Curves on figure 6.10, the detection levels are, as desired, perfectly aligned by the calibration procedure for each VFAT.

The S-Curves also allow a more detailed analysis of the VFATs and the positions on the GEB. As a matter of fact, some VFATs with a good threshold scan reveal some dysfunctions as, for example, the VFAT on position 2. Even if the threshold scan is correct and not too noisy, the S-Curves by channel reveals that the channel 77 and 78 are dead. It is important to note that the problem could come from the VFAT or from the position on the GEB. It is thus necessary to either test several numbers of dispositions of the VFATs on the GEB, or test them on a well defined GEB (from which the characteristic of the positions is known). Hopefully, a VFAT or a GEB position having a few unusable channels is not dramatic for the GE1/1 project, thanks to the redundancy of the muons tracker. These unusable channels can be masked by setting a bit in their channels registers not to perturb the measurements. Figure 6.10 allows a human eye to determine if some channels are unusable. However, given the number of VFATs to be tested for GE1/1, it is preferable to automatize the detection of bad channels. The CDF fit is used for this. Figure 6.11 shows the mean and the standard deviation of the fitted CDF function for the VFAT discussed above (position 2 on figure 6.10).

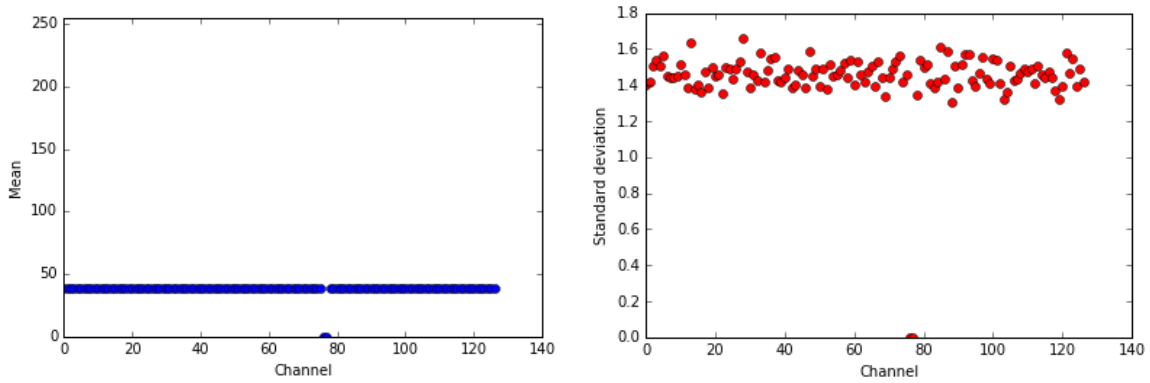

(a) Mean (b) Standard deviation

Figure 6.11: Parameters of the cumulative distribution functions fitted on the S-Curve of the VFAT on the position 2 as a function of the VFAT channel number.

From these results, a mechanism of detection can be implemented. A dead channel appears with a 0 mean and a 0 standard deviation. An unaligned channel appears with a divergent mean and a noisy channel appears with a divergent standard deviation. Furthermore, the fitted CDF quantifies these miss alignments and divergent standard deviations, making possible objective comparisons and quantitative analyses.

This example shows the importance of using the threshold scan and the S-Curve with their fit, because both could bring useful information. These steps have been implemented in the quality control procedure of the GE1/1 VFAT production.

Chapter 7

Noise characterization

Once the analysis of the GEB is done without detector, the system has to be tested connected to the detector. Even if the detector is kept shut down, it will introduce some noise as it will be shown in this chapter.

The script is thus run with the usual disposition (only the VFATs equipped with TP573650 voltage regulators and with the new firmware) on the lateral columns. The threshold scans and the S-curves obtained are presented for this set-up on figure 7.1 and 7.2.

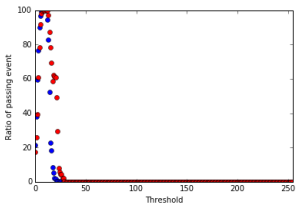

Position 0

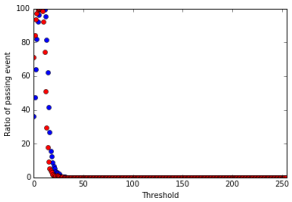

Position 16

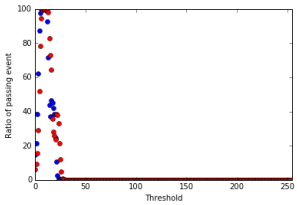

Position 1

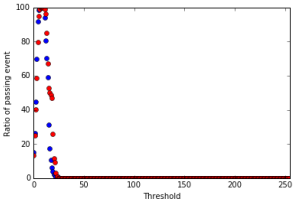

Position 17

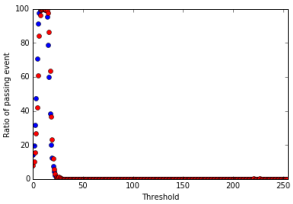

Position 2

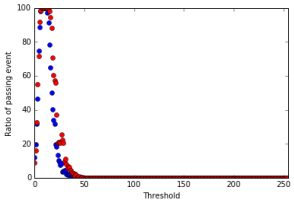

Position 18

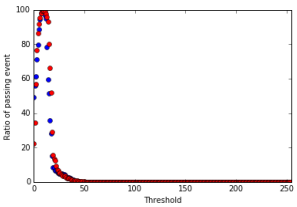

Position 3

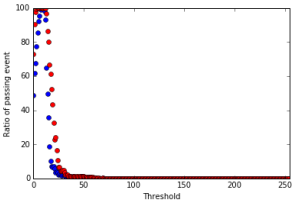

Position 19

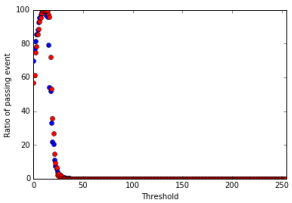

Position 4

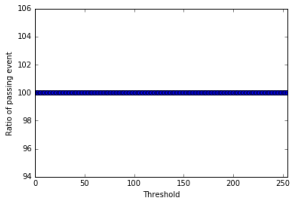

Position 20

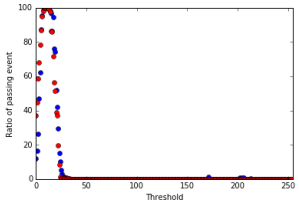

Position 5

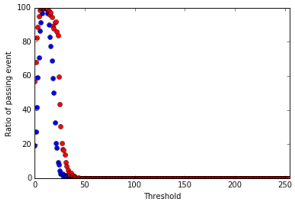

Position 21

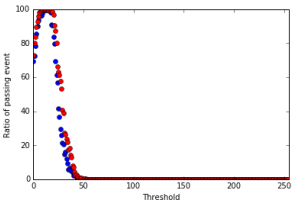

Position 6

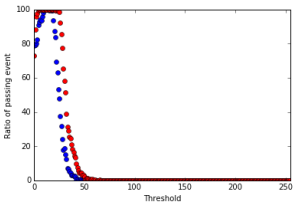

Position 22

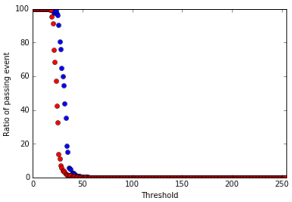

Position 7

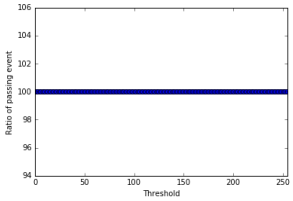

Position 23

Figure 7.1: Threshold scans of the VFATs connected to the detector.

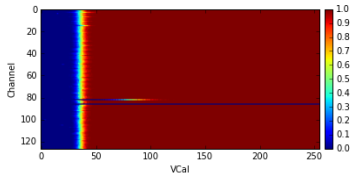

Position 0

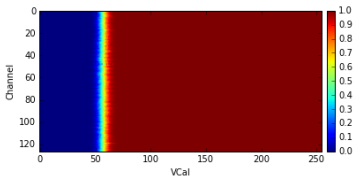

Position 16

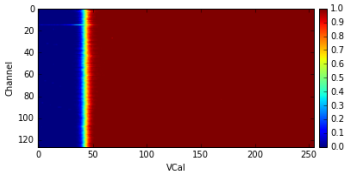

Position 1

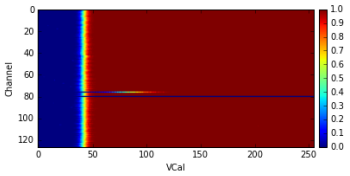

Position 17

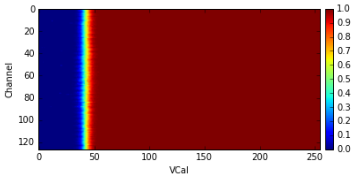

Position 2

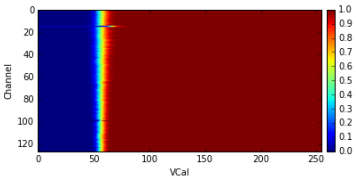

Position 18

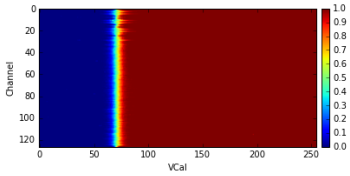

Position 3

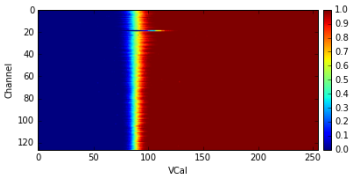

Position 19

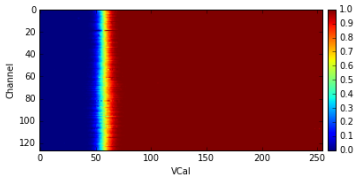

Position 4

DEAD POSITION

Position 20

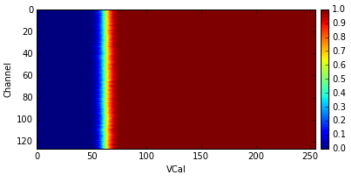

Position 5

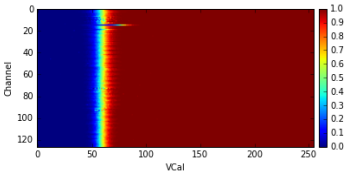

Position 21

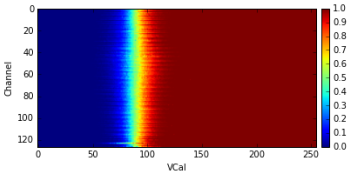

Position 6

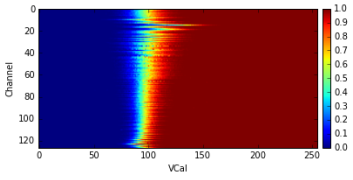

Position 22

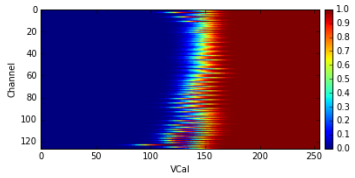

Position 7

DEAD POSITION

Position 23

Figure 7.2: S-Curves of the VFATs connected to the detector.

Immediately, an increase in the noise can be observed by the wider threshold scan. The closer the VFATs to the wide side of the GEB, the higher the noise. The detector thus introduces a non-uniform noise on the VFATs along the GEB. The first question is then to understand what changes on the detector between the short end and the wide end. In fact, the answer is in the question. As seen previously, the readout board is divided in 8 sectors in length, with a size from 11 cm at the short end to 19 cm at the wide end, and 3x128 channels in width. The channels on the wide end have thus a bigger area than the ones on the short end [6]. The designers of the analog circuit in the VFAT (pre-amplifier and comparator) have determined that the output noise, expressed in Equivalent Noise Charge (ENC), is proportional to the capacitance of the input channel [12, 15]:

$$ENC = 400e + X \;\; e^-/pF \tag{7.1}$$

with X depending on the pre-amplifier current. Since the capacitance is proportional to the area, this equation confirms the theory that the the noise increase results, at least partially, from the increasing area of the strips.

In order to check if the increase in the strips area is the only cause of the observed increasing noise, the theoretical noise will be compared to the noise of the VFATs connected to the detector. First, the theoretical noise is computed with the equation 7.1. Secondly, the noise will be extracted from the measurements. Finally, the two noises are compared.

7.1 Theoretical Noise

The equation 7.1 computes the ultimate best (lower) noise in number of electrons that the VFAT can reach. The constant term is the noise created by the analog circuit of the VFAT. The second term computes the noise degradation caused by a capacitance connected at the input of the analog circuit. As mentionned above, it is proportional to the current of the pre-amplifier: a larger current induces a smaller noise. For the case of the VFAT in the GE1/1 project, an optimal power consumption on noise ratio is reached for a pre-amplifier current of 450 μA, which leads to $X = 50$ [15].

It is thus necessary to know the capacitance of the strips of the triple-GEM to compute the theoretical noise.

7.1.1 Capacitance determination

The predicted capacitance of the triple-GEM tracks is 23 pF for the biggest ones. A diminution of 30 to 50% is expected for the smaller channels. Since the prediction are not precise, the capacitance of the tracks has been measured directly on the detector. Table 7.1 presents the measurements along with the corresponding theoretical noise.

Positions	Capacitance	ENC
0-8-16	14.5 pF	1125 e-
1-9-17	12 pF	1000 e-
2-10-18	17 pF	1250 e-
3-11-19	17.5 pF	1275 e-
4-12-20	18.7 pF	1335 e-
5-13-21	20 pF	1400 e-
6-14-22	22.2 pF	1510 e-
7-15-23	27.5 pF	1775 e-

Table 7.1: Measured capacitances of the tracks and their equivalent theoretical noise.

7.2 Measured Noise

The measured noise is extracted from the S-Curve. However, the S-Curve parameters have so far been expressed in VFAT units. Therefore, the calibration pulses need to be calibrated to convert the charge in fC or number of electrons.

7.2.1 VFAT unit conversion

To determine the charge in voltage of a pulse sent by the calibration module, the analog to digital converter (ADC) of the VFAT is used. The calibration module sends the pulse as a difference between two voltages. Figure 7.3 shows these two voltages as a function of the value of the calibration pulse register.

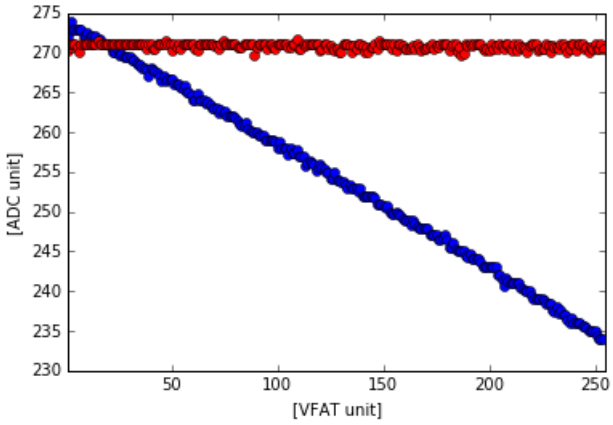

Figure 7.3: Differential voltage sent by the calibration module.

At this point, the voltages are expressed in "ADC counts". The ADC is a "TI MSP430-EZ430" and its conversion from "ADC count" to voltage is given by:

$$V = 0.0029x + 0.0093 \tag{7.2}$$

which gives the conversion line from "VFAT units" to "volt" presented on figure 7.4.

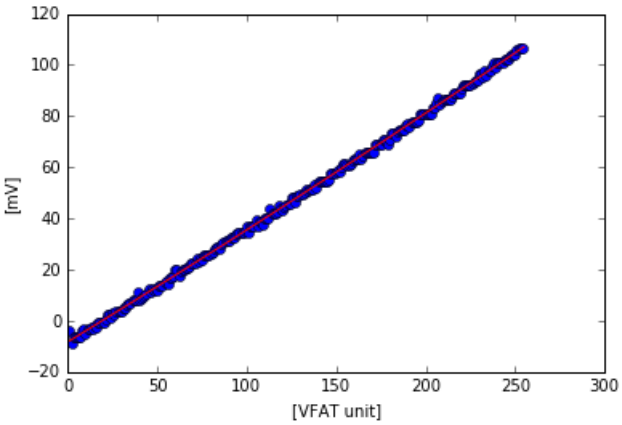

Figure 7.4: Conversion from VFAT Unit to mV.

The calibration module sends a pulse of a certain voltage on a capacitance of 100 fF at the input of the channels as shown on figure 7.5.

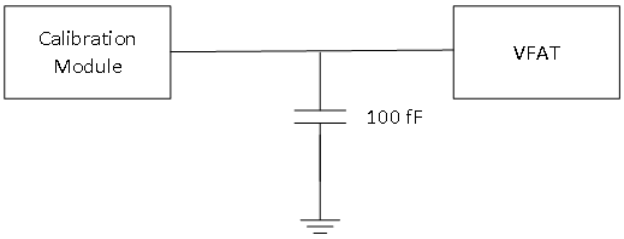

Figure 7.5: Capacitance between the VFAT and the calibration module.

Finally, the charge in fC sent on the channels is thus determined by $Q = CV$. The results of the conversion for 6 VFATs are shown on figure 7.6.

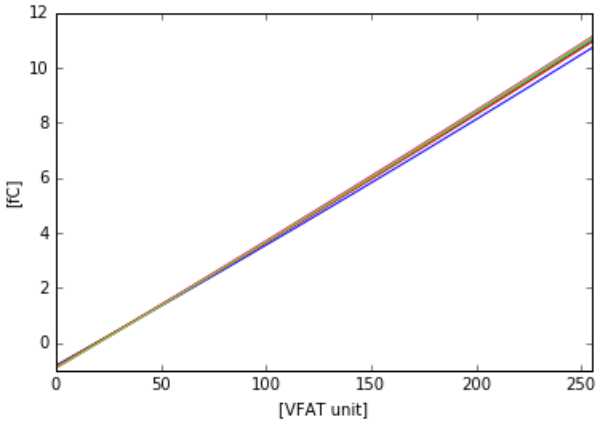

Figure 7.6: Comparison of the conversion from VFAT Unit to fC for 6 VFATs.

The fact that all the conversion lines are close to each other allows to use an average conversion for all the VFATs:

$$VCal[fC] = -0.919 + 0.04668 VCal[VFATUnit] \tag{7.3}$$

Then the charge in electron is determined by dividing the charge in coulomb by the elementary charge ($1.60217 \cdot 10^{-19}$) .

7.2.2 Extraction of the noise from the S-Curve

Once the conversion equation is known, the noise of a channel based on the S-Curve can be determined using the standard deviation of the fitted CDF [9, 15, 16] as shown on figure 7.7.

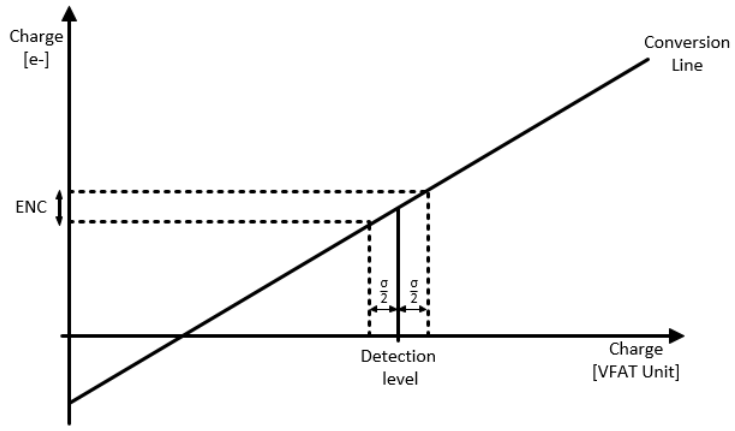

Figure 7.7: Determination of the ENC using the conversion line and the standard deviation.

By applying this method on the measurements with and without being connected to the detector the following table is obtained:

Pos.	ENC (w/o detector)	ENC (w/ detector)	Pos.	ENC (w/o detector)	ENC (w/ detector)
0	430.5 e-	1073 e-	16	453 e-	1322 e-
1	432 e-	1009 e-	17	430 e-	975 e-
2	431 e-	1228 e-	18	417 e-	1359 e-
3	435 e-	1256 e-	19	430.5 e-	1712 e-
4	428.5 e-	1683 e-	20		
5	447 e-	1557 e-	21	441 e-	1695 e-
6	421 e-	3411 e-	22	418 e-	3146 e-
7	441 e-	3009 e-	23		

Table 7.2: Measured noise from the S-Curves

The noise determination from the S-Curve has been implemented in the code "*read_and_plot.py*", which now outputs the noise in e- and in fC for the scanned VFATs.

7.3 Comparaison and Discussion

In the case of the VFATs not connected to the detector, the noise behaves as predicted. It is constant and its value is close to the 400e- predicted. The VFATs not connected are thus operating at the lowest noise level achievable. In the case of the VFATs connected to the detector, table 7.3 compares the theoretical and the measured noise.

Pos.	Theoretical ENC	Measured ENC	Ratio	Pos.	Theoretical ENC	Measured ENC	Ratio
0	1125 e-	1073 e-	0.95	16	1125 e-	1322 e-	1.18
1	1000 e-	1009 e-	1.01	17	1000 e-	975 e-	0.98
2	1250 e-	1228 e-	0.98	18	1250 e-	1359 e-	1.09
3	1275 e-	1256 e-	0.99	19	1275 e-	1700 e-	1.33
4	1335 e-	1683 e-	1.26	20			
5	1400 e-	1557 e-	1.11	21	1400 e-	1695 e-	1.21
6	1510 e-	3411 e-	2.26	22	1510 e-	3146 e-	2.08
7	1775 e-	3009 e-	1.70	23			

Table 7.3: Comparison of the measured noise and the theoretical noise for the VFATs connected to the detector.

The noise added by the detector seems to fit with the measurements for the small end off the GEB. But the closer to the wide end, the higher the difference between the theoretical noise and the measured one. That indicates the increased capacitance of the strips are not the only reason for the noise increase when the VFATs are connected to the detector: another non-homogeneous noise is induced. This noise seems to be particularly high for the 2 rows of VFATs on the wide side of the GEB.

To valid that the remaining noise is induced by the detector and not by the Opto-hybrid, the GEB has been physically shifted in length to align its position 0 with the connector in which the largest strips of the readout board are plugged. The results of the scan on a VFAT connected on this position show no modification on the noise. This noise is thus induced by the larger strips independently of the VFAT position on the GEB.

Conclusion

In the framework of the CMS muon tracker upgrade for the HL-LHC project, we have developed a toolkit including firmware and software routines to control the front-end VFAT ASIC from a FPGA-based board located on the new triple-GEM detector.

Initially, the purpose of this master thesis was to implement a procedure which had the precise and defined objective of realizing an automated calibration of the VFATs. That procedure turned out to be very useful on many other aspects. As a matter of fact, it has permitted the discovery of unexpected problems on the VFATs. In addition, its systematic and automated use has allowed, in most cases, to determine the sources of these problems. A notable example could be the noise pattern of the detector central column or the extra noise induced by the detector. These noises could have appeared as random if a less systematic approach would have been taken.

As a result, following the first objective, we have developed and implemented the full calibration procedure of the CMS VFAT chip. The routines we provide are fully automatized, which is an asset for the CERN operators who will have to test nearly 3500 VFAT chips for the GE1/1 project. From now on, the calibration routine will indeed serve as the official quality control procedure of these chips. Based on the functional test features of the VFAT chip, the threshold scan and the S-Curve, the proposed procedure brings consistency to the comparator threshold over the whole VFAT chip. Beside, it detects noisy and dead channels. At the end, the routine saves the relevant VFAT parameters and the main test results in a file, which will be recorded in the general CMS database to serve as a reference when the detector will be operating at LHC.

In addition, the proposed calibration routine has allowed to test systematically the VFAT and the GEB board equipping the ULB CMS GE1/1 development set-up. This has raised several unexpected observations like non-working positions on the GEB, voltage regulator noise, I^2C clock induced noise...

The outcomes of this work have been multiple. First, we have identified and solved several noise sources in the system. We have also demonstrated for the very first time that the VFAT chip is working exactly as expected, reproducing the ultimate noise when the detector is not connected. We have also shown that the noise follow the expected formula when the system is connected to the VFAT, at least for the smallest strips of the GEM detector.

Currently, the proposed routine starts to be used at CERN and the first measurements from the CERN set-up are coming out confirming the results obtained in this work. Eventually, a larger statistics will help to identify the remaining noise issues.

Appendix A

Detailed Decomposition Of A GE1/1 Detector

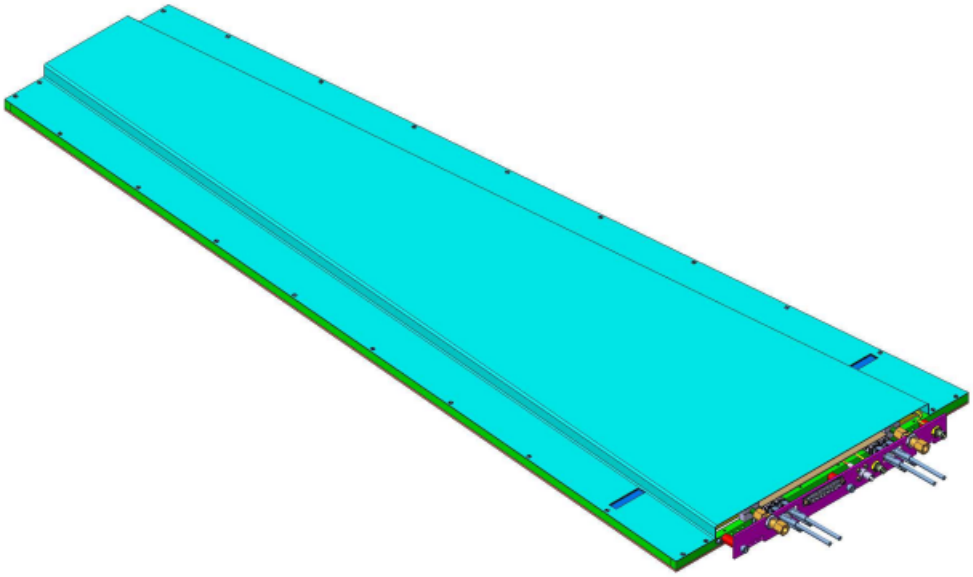

Figure A.1: Overall view of the detector [6].

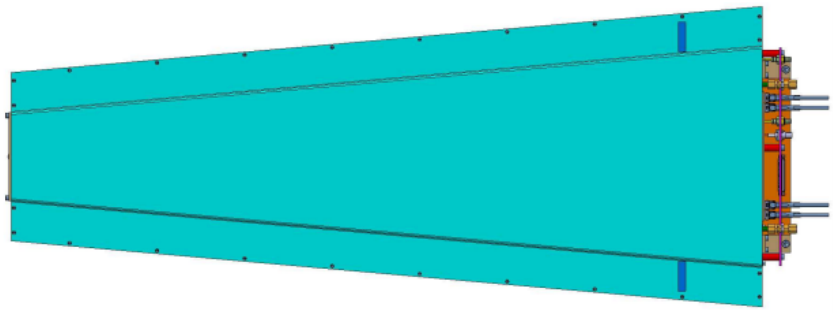

Figure A.2: Top view of the detector [6].

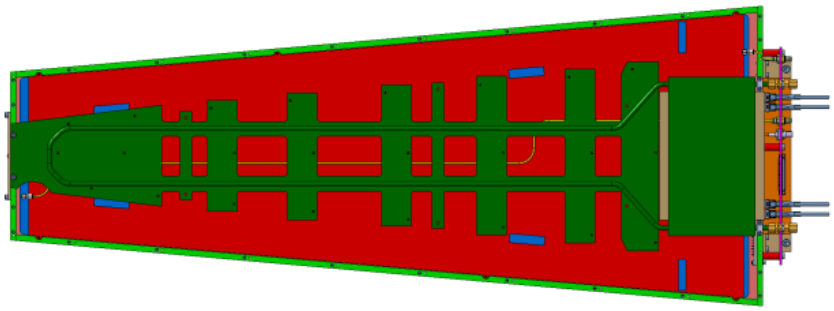

Figure A.3: Cooling circuit [6].

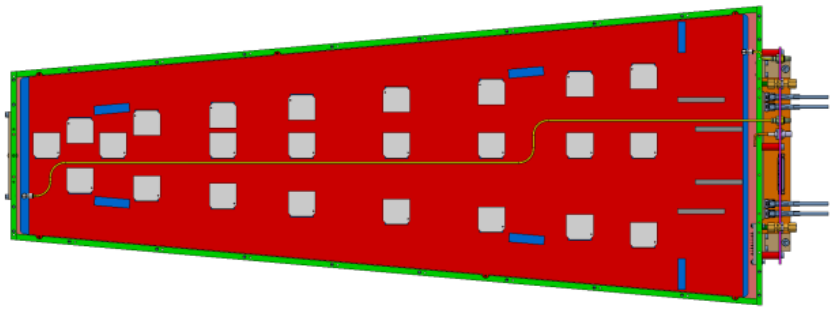

Figure A.4: GEB with the VFAT connected [6].

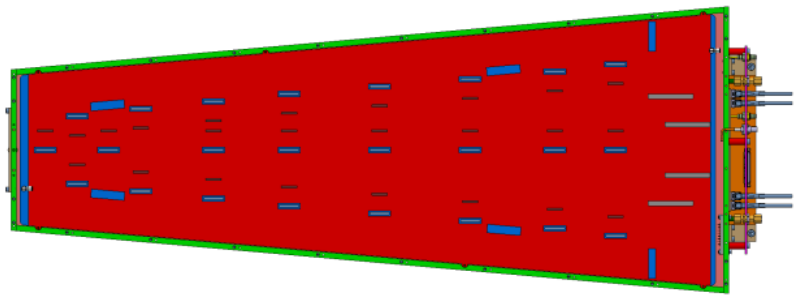

Figure A.5: GEM Board [6].

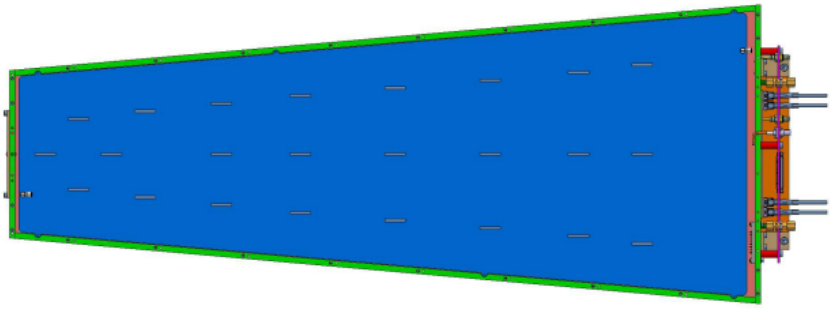

Figure A.6: Readout Board [6].

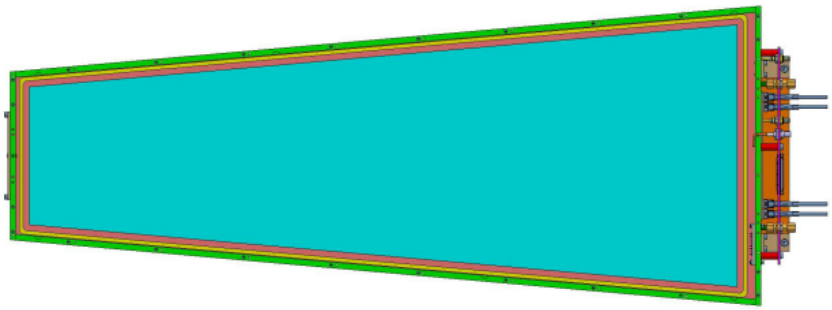

Figure A.7: GEM foil [6].

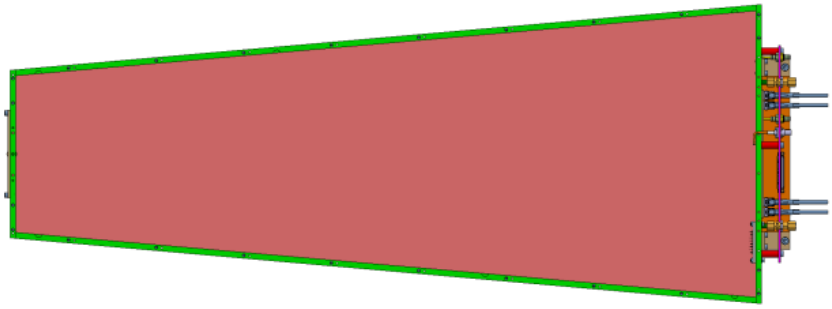

Figure A.8: Drift electrode of the triple-GEM [6].

List of Figures

List of Tables

Bibliography

[1] Cern : Official website. `http://home.cern/` Accessed: 2015-05-15.

[2] Public cms documents. `https://cms-docdb.cern.ch/cgi-bin/PublicDocDB/DocumentDatabase` Accessed: 2015-05-15.

[3] P. Aspell. *VFAT2 - Operating Manual*. 2006.

[4] The CMS Collaboration. *TECHNICAL PROPOSAL FOR THE UPGRADE OF THE CMS DETECTOR THROUGH 2020*. 2011.

[5] The CMS Collaboration. *Observation of a new boson at a mass of 125 GeV with the CMS experiment at the LHC*. 2012.

[6] The CMS Collaboration. *CMS TECHNICAL DESIGN REPORT FOR THE MUON ENDCAP GEM UPGRADE*. 2015.

[7] The CMS GEM collaboration. *Status of the Triple-GEM project for the upgrade of the CMS Muon System*. 2013.

[8] The LHCb Collaboration. *LHCb Tracker Upgrade Technical Design Report*. 2014.

[9] The TOTEM Collaboration. *The TOTEM Experiment at the CERN Large Hadron Collider*. 2008.

[10] Lyndon Evans and Philip Bryan. *LHC machine.Journal of Instrumentation*. 2008.

[11] Baptiste Herregods. *Contribution à l'étude de détecteurs équipés de GEM pour les upgrades du spectromètre à muons de CMS*. 2015.

[12] J. Kaplon and W. Dabrowski. *Fast CMOS Binary Front End for Silicon Strip Detectors at LHC Experiments*. 2005.

[13] Lorenzo Foa Paraskevas Sphicas Darin Acosta Albert De Roeck Lucia Silvestris Avi Yagil Michel Della Negra, Alain Herve. *CMS Physics, Technical Design Report, Volume I: Detector Performance and Software*. 2006.

[14] V. Bobillier S. Haas M. Hansen M. Joos P. Vichoudis, S. Baron and F. Vasey. *The Gigabit Link Interface Board (GLIB), a flexible system for the evaluation and use GBT-based optical links*. 2010.

[15] P.Chalmet J.Kaplon K.Kloukinas H.Mugnier W.Snoeys P.Aspell, G.Anelli. *VFAT2 : A front-end system on chip providing fast trigger information, digitized data storage and formatting for the charge sensitive readout of multi-channel silicon and gas particle detectors.* 2007.

[16] W.Bialasa J.Kaspara J.Kopalc J.Petäjäjärvid E.Radicionie J.Roueta W.Snoeysa P.Vichoudisa P.Aspell, V.Avatia. *The VFAT Production Test Platform for the TOTEM Experiment*. 2008.

[17] Michael Tytgat. *Technical and Political Status of the CMS Muon Chambers Upgrade*. 2006.

[18] VadaTech. *MicroTCA Overview - A Brief Introduction to Micro Telecommunications Computing Architecture Concepts*. 2014.

[19] E. Verhagen. *Development of the new trigger and data acquisition system for the CMS forward-muon spectrometer upgrade*. 2015.